Lung Cancer

11

Yoshiharu Ohno, Hisanobu Koyama, Julien Dinkel, and Christian Hintze

CONTENTS

KEY POINTS

Since the publication of the Radiologic Diagnostic Oncology Group Report (RDOG) in 1991, the clinical application of pulmonary magnetic resonance (MR) imaging to patients with lung cancer has been limited. MDCT is much more widely available for staging of lung cancer in clinical situations. Currently, FDG-PET or PET/CT is the only modality that reveals biological glucose metabolism of lung cancer, and ventilation and/ or perfusion scintigraphy is the only modality that demonstrates pulmonary function. However, recent advances of MR systems and utilization of contrast media make it possible to overcome the limitation of pulmonary MR imaging. Therefore, in the last several years, several investigators have demonstrated the significant comprehensive potential of MR imaging to substitute for MDCT and nuclear medicine examinations in lung cancer patients. Currently, MR imaging in lung cancer patients can be applied for (1) detection of pulmonary nodules; (2) characterization of solitary pulmonary nodules; and (3) assessment of TNM classification in routine clinical practice. We believe that further basic studies, as well as clinical applications of newer MR techniques, will play an important role in the future management of patients with lung cancer including MRI.

Y. Ohno, MD, PhD
Director of Diagnostic and Functional Imaging Research, Director of Thoracic Radiology, Associate Professor of Radiology, Department of Radiology, Kobe University Graduate School of Medicine, 7-5-2 Kusunoki-cho, Chuo-ku, Kobe, 650-0017, Japan

H. Koyama, MD, PhD
Department of Radiology, Kobe University Graduate School of Medicine, 7-5-2 Kusunoki-cho, Chuo-ku, Kobe, 650-0017, Japan

C. Hintze, MD
German Cancer Research Center (DKFZ), Im Neuenheimer Feld 280, 69120 Heidelberg, Germany

J. Dinkel, MD, MSc
German Cancer Research Center (DKFZ), Im Neuenheimer Feld 280, 69120 Heidelberg, Germany

11.1 Introduction

Lung cancers are the most common cause of cancer-related death in the Western world, Japan, and South Korea. Non-small cell lung carcinoma (NSCLC) accounts for approximately 80% of all lung cancers, with small cell lung carcinoma (SCLC) accounting for the remainder. Despite major efforts aimed at improving survival during recent years, survival remains dismal at 14% for all stages. Imaging techniques currently are essential for the diagnosis, staging and follow-up of patients with lung cancer. The diagnosis of lung cancer has relied on findings on chest radiographs (CXRs) and detection of cells in sputum or biopsy specimens. Perhaps even more important, however, are specific findings on chest computed tomography (CT) and metabolic information on positron emission tomography with 2-[fluorine-18]-fluoro-2-deoxy-D-glucose (FDG-PET) or FDG-PET co-registered or integrated with CT (co-registered or integrated FDG-PET/CT). Moreover, the staging and follow-up of lung cancer have relied more on CT, FDG-PET and/or FDG-PET/CT than on chest radiography. The goal of diagnosis and management of pulmonary nodules is to bring promptly to surgery all patients with operable malignant nodules while avoiding unnecessary thoracotomy for patients with benign lesions. It is therefore of the utmost importance to differentiate malignant from benign nodules in the least invasive manner and to make as specific and accurate diagnosis as possible. In addition, the preliminary goal of pre-therapeutic assessment of lung cancers is to avoid unnecessary surgery for patients with locally unresectable tumors and/or nodal or metastatic disease because the strongest prognostic indicator for survival in lung cancer is whether or not the tumor is resectable.

Currently, CT is considered to be the most widely applicable modality for evaluation of lung cancer, and a major breakthrough in CT technology has been the introduction of multidetector-row CT (MDCT), in which detector rows are exposed simultaneously. The performance of MDCT compared with single-detector CT is enhanced by a factor approximately equal to the number of rows. In addition, FDG-PET or PET/CT qualifies as another important innovation in lung cancer imaging. Standard imaging techniques are based on differences in the structure of tissues, whereas FDG-PET or PET/CT can show the enhanced glucose metabolism of lung cancer cells. For these reasons, MR imaging has been utilized for only a few cases, such as superior sulcus (Pancoast's) tumor, mediastinal invasion and chest wall invasion since 1991, when the Radiologic Diagnostic Oncology Group (RDOG) reported no significant difference in the diagnostic capability of CT and conventional T1-weighted imaging for the staging of lung cancer except for mediastinal invasion (Webb et al. 1991). However, recent advances in MR imaging techniques and utilization of contrast media have resulted in further improvement of the image quality and diagnostic capability of MR imaging for lung cancer patients.

In this chapter we describe the utility and capability of MR imaging for (1) detection of pulmonary nodules, (2) characterization and management of pulmonary nodules, and (3) assessment of tumor-node-metastasis (TNM) stages in lung cancer patients.

11.2 Detection of Pulmonary Nodules

A pulmonary nodule is radiologically defined as an intraparenchymal lung lesion that is less than 30 mm in diameter and is not associated with atelectasis or adenopathy (Tuddenham 1984). While one in 500 CXRs shows a lung nodule, 90% of these nodules are incidental radiological findings, detected accidentally on CXRs obtained for unrelated diagnostic workups. More than 150,000 patients per year in the United States present their physicians with the diagnostic dilemma of a pulmonary nodule. This number has increased even further due to incidental findings of lung nodules on chest CT (Tuddenham 1984). The devastating effect of lung cancer is directly associated with its delayed presentation. Patients with the best prognosis are those with stage IA disease, although approximately one half of all lung cancers unfortunately show extrathoracic spread at the time of diagnosis. Timely and accurate detection and diagnosis of the etiology of pulmonary nodules are therefore essential for making it possible for patients with malignancy to be cured.

Spiral CT or MDCT can be considered the current gold standard for the detection of lung nodules (Davis 1991; Costello 1994; Henschke et al. 2001; Schaefer-Prokop and Prokop 2002; Swensen et al. 2005; Bach et al. 2007). However, repeated follow-up CT examinations for detection of pulmonary metastases may be undesirable, especially for young patients, because of radiation exposure. Although radiation exposure is usually no major issue for cancer patients and low-dose CT techniques have been proved feasible to reduce the radiation dose, MR imaging does not require any ionizing radiation at all. It would therefore be helpful if MR imaging could be used for the detection of pulmonary nodules without administration of contrast media.

Several investigators have addressed this issue by using various sequences with 1.5 T and 3.0T scanners since 1997. However, patient-related motion artifacts, susceptibility artifacts from the lungs and inferior spatial and temporal resolution as compared with those of CT reduce the quality of MR images of the lungs (Kersjes et al. 1997; Vogt et al. 2004; Schroeder et al. 2005; Luboldt et al. 2006; Bruegel et al. 2007; Regier et al. 2007; Yi et al. 2007). All these studies assessed the detection rate (sensitivity) for pulmonary nodules, mainly pulmonary metastases, which was verified by single-helical CT or MDCT. The sensitivities for nodules equal to or less than 5 mm in diameter were reportedly less than 45%, although various sequences such as electrocardiograph (ECG)-triggered proton density weighted (PDW) or T2-weighted turbo spin-echo (SE), ECG-triggered PDW black-blood-prepared half-Fourier single-shot turbo SE (HASTE), respiratory-triggered T2-weighted short-inversion-time inversion recovery (STIR) turbo SE, pre- and post-contrast enhanced volumetric interpolated 3D gradient-echo (VIBE), T2-weighted triple inversion black blood turbo spin-echo, etc. were tested with nodules equal to or more than 5 mm section thickness on 1.5 T or 3.0 T scanners (Kersjes et al. 1997; Vogt et al. 2004; Schroeder et al. 2005; Luboldt et al. 2006; Bruegel et al. 2007; Regier et al. 2007; Yi et al. 2007). On the other hand, sensitivities for nodules equal to or more than 5 mm and less than 11 mm in diameter were reportedly between approximately 85% and 95%, and those for nodules with a diameter of more than 10 mm were more than 95% in these studies (Kersjes et al. 1997; Vogt et al. 2004; Schroeder et al. 2005; Luboldt et al. 2006; Bruegel et al. 2007; Regier et al. 2007; Yi et al. 2007). Therefore, when considering the various guidelines for management of pulmonary nodules (Kersjes et al. 1997; Vogt et al. 2004; Schroeder et al. 2005; Luboldt et al. 2006; Bruegel et al. 2007; Regier et al. 2007; Yi et al. 2007), MR imaging on 1.5 T and 3.0 T may have potential for the detection of or screening, without ionizing radiation exposure, for pulmonary nodules which are considered to need further intervention and treatment (Figs. 11.1–11.3), (Table 11.1). In addition,

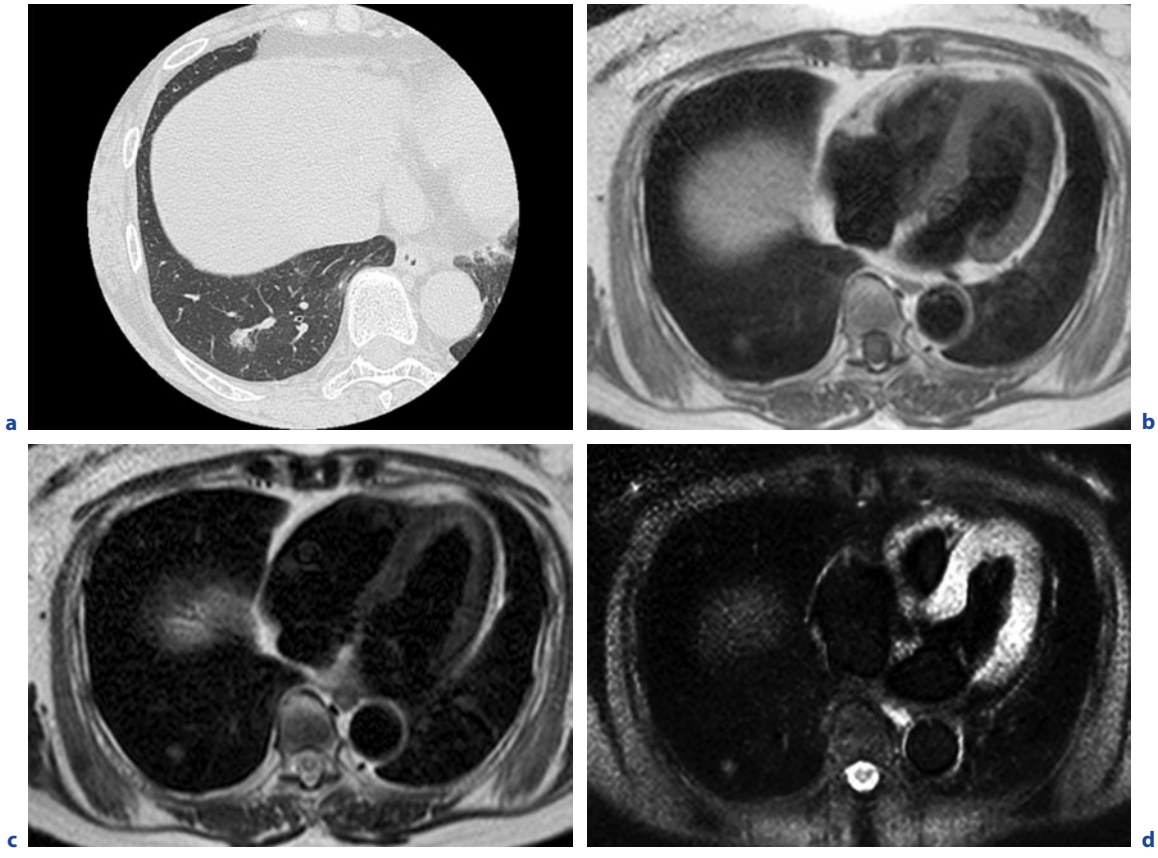

Fig. 11.1a–d. A 71-year-old female with adenomatous hyperplasia in the right lower lobe. Thin-section CT indicates ground-glass attenuation in the right lower lobe (**a**). Black-blood T1-weighted turbo SE (**b**), T2-weighted turbo SE (**c**) and STIR turbo SE (**d**) images show a nodule as, respectively, low, intermediate and high signal intensity in the right lower lobe


a

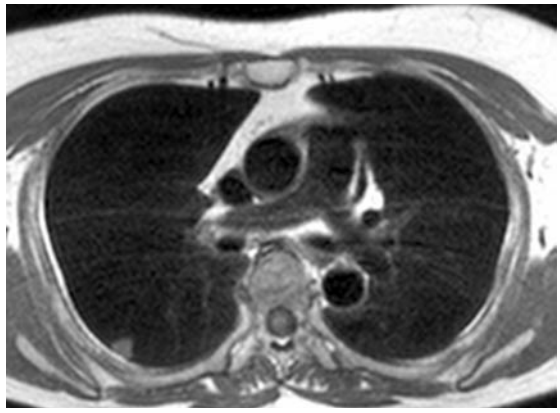
b

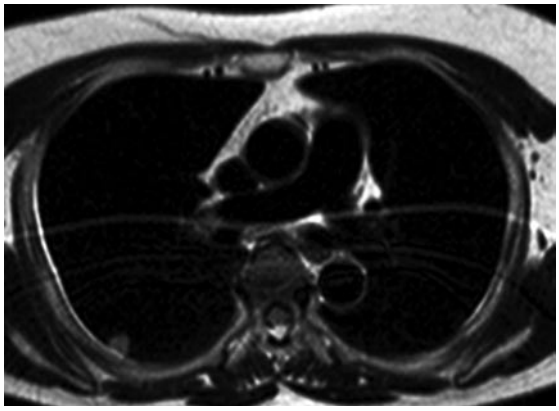
c


d

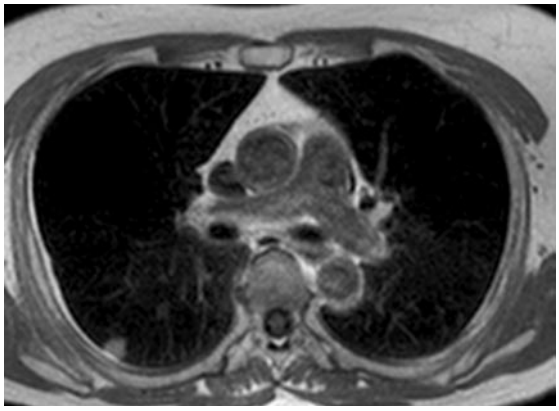
e

Fig. 11.2a–e. A 56-year-old female with adenocarcinoma in the right lower lobe. Thin-section CT shows a solid nodule in the right lower lobe (**a**). Black-blood T1-weighted turbo SE (**b**), T2-weighted turbo SE (**c**) and STIR turbo SE (**d**) images show nodule as, respectively, low, low or intermediate and high signal intensity in the right lower lobe. Post-contrast black-blood T1-weighted turbo SE image (**e**) showed homogeneous enhancement of nodule

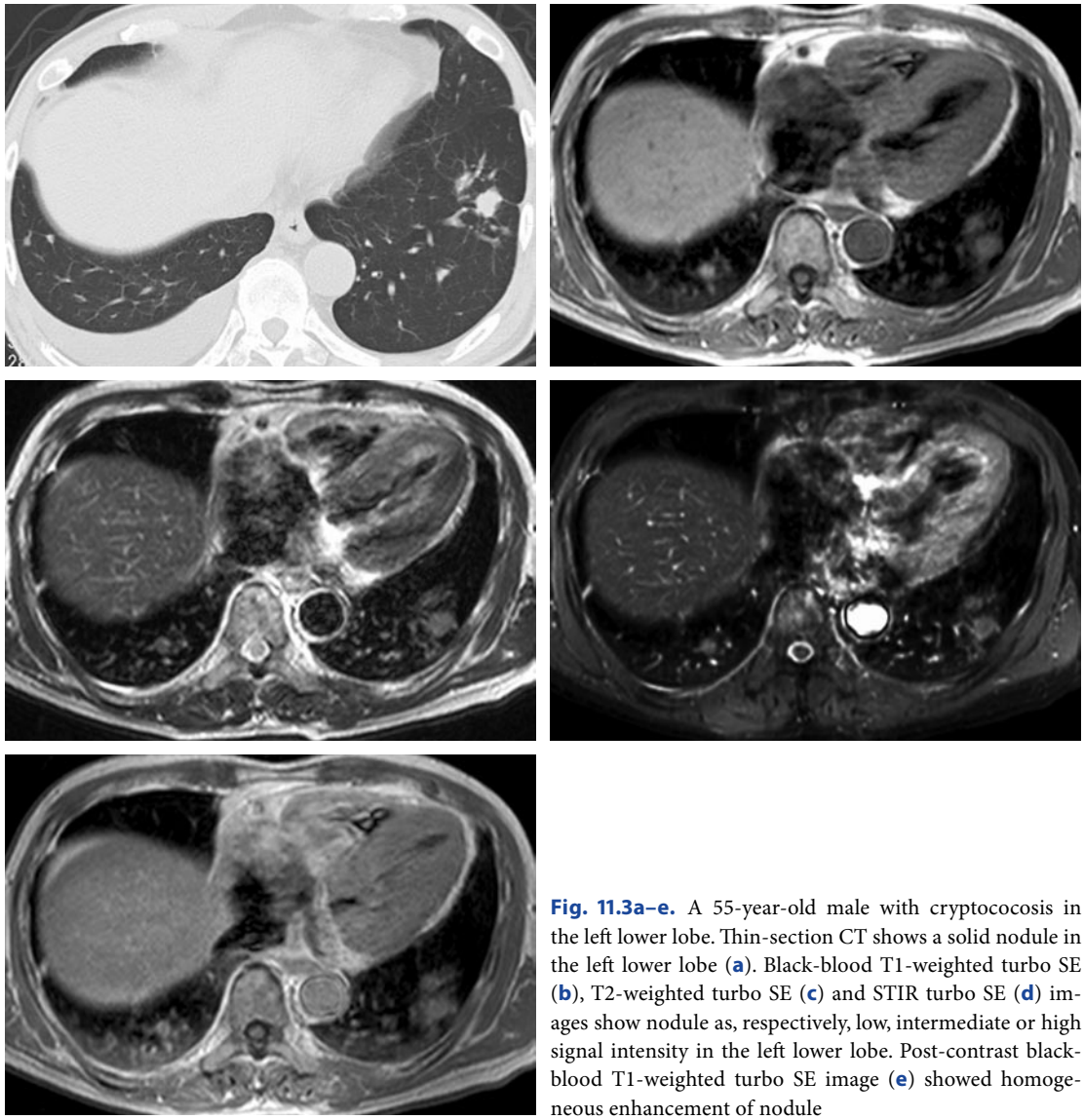

Fig. 11.3a–e. A 55-year-old male with cryptococosis in the left lower lobe. Thin-section CT shows a solid nodule in the left lower lobe (**a**). Black-blood T1-weighted turbo SE (**b**), T2-weighted turbo SE (**c**) and STIR turbo SE (**d**) images show nodule as, respectively, low, intermediate or high signal intensity in the left lower lobe. Post-contrast black-blood T1-weighted turbo SE image (**e**) showed homogeneous enhancement of nodule

Table 11.1. Recommended MR protocol for nodule detection and characterization

No.	Recommended sequence	TR (ms)	TE (ms)	FA (°)	Matrix	Respiration	Suggestion
1	Pre-contrast-enhanced ECG-gated T1W-SE or TSE	1 <R-R>	15–25	N/A	256 × 256	RT or RG	
2	ECG- and respiratory-gated T2W-TSE	2 or 3 <R-R>	90–100	N/A	256 × 256	RT or RG	ETL should be less than 15
3	Respiratory-gated STIR TSE	Up to respiratory cycle	15	N/A	256 × 256	RG	ETL should be less than 5, if sequentially-reordered phase encoding scheme is used
4	Dynamic MRI by using 3D ultra-fast T1-GRE	2.4–2.7	0.6–0.7	20–40	128 × 128	BH	Dynamic MR images should be obtained every 1.1 s after contrast media injection
	Dynamic MRI by using ECG-gated T1W-SE	150-1 <R-R>	10–15	N/A	128 × 128–256 × 256	BH	Dynamic MR images should be obtained at 0, 1, 2, 3, 4, 5, 6 and 8 min after contrast media injection
5	Post contrast-enhanced ECG-gated T1W-SE or TSE	1 <R-R>	15–25	N/A	256 × 256	RT or RG	

SE: spin-echo, TSE: turbo spin-echo, GRE: gradient echo, TR: repetition time, TE: echo time, FA: flip angle, RT: respiratory-trigger, RG: respiratory-gated, ETL: echo train length

further improvements of MR systems and sequences can be expected to enable pulmonary metastasis surveillance and/or lung cancer screening as well as whole-body MR screening or staging in the near future.

11.3 Characterization and Management of Pulmonary Nodules or Masses on MR Imaging

Since the pulmonary nodule is one of the most common findings on chest radiographs and CT, it is important to differentiate malignant from benign nodules in the least invasive way and to make as specific and accurate diagnosis as possible. Investigators have used CT, MR imaging and FDG-PET or PET/CT to evaluate the radiological features, relaxation time, blood supply and metabolism of pulmonary nodules to differentiate malignant from benign nodules with promising results. (Table 11.1).

11.3.1 Conventional T1-Weighted and T2-Weighted MRI Without and With Contrast Media

Characterization of the primary tumor on CT and MR imaging is based on the imaging features of the nodule or mass itself and its relationship to the pleura, chest wall, airways, and mediastinum, as well as its relative enhancement by contrast media. Historically, non-contrast-enhanced MR imaging has shown limited potential for characterizing peripheral lung nodules and masses and identifying benign nature of nodules due to the low intrinsic signal intensity of the lung parenchyma, the relatively poor spatial resolution and patient-related motion artifacts (Caskey et al. 1990; Feuerstein et al. 1992; Kono et al. 1993; Kersjes et al. 1997; McLoud and Swenson 1999). In general, many pulmonary nodules, including lung cancers, pulmonary metastases and low-grade malignancies such as carcinoids and lymphomas are demonstrated as low or intermediate signal intensities on T1-weighted images and

as slightly high intensity on T2-weighted images when SE or turbo SE sequences are used (Caskey et al. 1990; Feuerstein et al. 1992; Kono et al. 1993; Kersjes et al. 1997; McLoud and Swensen 1999) (Fig. 11.2). If the pulmonary nodule is less than 30 mm in diameter, malignant pulmonary nodules within the tumor usually how no macroscopic necrosis (Caskey et al. 1990; Feuerstein et al. 1992; Kono et al. 1993; Kersjes et al. 1997; McLoud and Swensen 1999). Although enhancement levels vary due to underlying microscopically determined pathologic conditions such as tumor angiogenesis, tumor interstitial spaces, the presence or absence of fibrosis, and scarring and necrosis within the tumor, malignant pulmonary nodules show homogeneous enhancement but at a variety of levels on T1-weighted images after administration of contrast media (Caskey et al. 1990; Feuerstein et al. 1992; Kono et al. 1993; Kersjes et al. 1997; McLoud and Swensen 1999). Consequently, when using pre- and post-contrast enhanced conventional T1-weighted images and T2-weighted images, clinicians in routine clinical practice often face a diagnostic dilemma in distinguishing malignant from benign pulmonary nodules such as organizing pneumonia, benign tumors and inflammatory nodules (Caskey et al. 1990; Feuerstein et al. 1992; Kono et al. 1993; Kersjes et al. 1997; McLoud and Swensen 1999) (Figs. 11.2 and 11.3). It has therefore been suggested that enhancement patterns or blood supply evaluated with dynamic contrast-enhanced MR imaging may be helpful for diagnosis and management of pulmonary nodules (Kono et al. 1993; Kusumoto et al. 1994; Hittmair et al. 1995; Gückel et al. 1996; Fujimoto et al. 2003; Ohno et al. 2002, 2004a; Schaefer et al. 2004, 2006; Kono et al. 2007; Donmez et al. 2007). However, it may be possible to diagnose several histological types of pulmonary nodules, such as bronchocele, tuberculoma, mucinous bronchioalveolar carcinoma (BAC), hamartoma and aspergilloma, on pre- or post-contrast enhanced T1-weighted images and T2-weighted image according to their specific MR findings.

11.3.1.1 Bronchial Atresia and Bronchocele

Bronchial atresia is a common focal pulmonary lesion, which can be diagnosed by using non-contrast enhanced T1- and T2-weighted images. Bronchial atresia is an uncommon anomaly characterized by focal obliteration of the bronchial lumen and the absence of communication between lobar, segmental or subsegmental bronchi and the central airway (Meng et al. 1978; Jederlinic et al. 1987; Finck and Milne 1988; Naidich et al. 1988; Bailey et al. 1990; Ko et al. 1998; Matsushima et al. 2002). Mucus secreted within the patent airways distal to the point of atresia accumulates in the form of a plug or bronchocele which appears as a pulmonary nodule or mass (Finck and Milne 1988; Naidich et al. 1988; Bailey et al. 1990; Ko et al. 1998; Matsushima et al. 2002). The MR image of bronchoceles reportedly appears as a branching lesion with high signal intensity on T1- and T2-weighted images due to the dilated mucus-filled bronchi and mucocele formation distal to the atelectatic segment (Finck and Milne 1988; Naidich et al. 1988; Bailey et al. 1990; Ko et al. 1998; Matsushima et al. 2002) (Fig. 11.4).

11.3.1.2 Tuberculoma

Tuberculomas, observed as well-defined nodules located mainly in the upper lobes, may appear after primary or reactivated tuberculosis. Calcification occurs in about 20%–30% of cases (Sochocky 1958). CT yields superior visualization of the calcifications and characteristics of the nodules. In rare cases, areas of diminished attenuation are seen, which represent caseous necrosis. The latter may be identified as tuberculoma, a nodule with a relatively low signal intensity in comparison with that of other pulmonary nodules on T2-weighted SE or turbo SE images (Sakai et al. 1992; Kono et al. 1993; Kusumoto et al. 1994; Parmar et al. 2000; Chung et al. 2000; Schaefer et al. 2006). In addition, several investigators have reported on typical MR findings of tuberculoma on post-contrast enhanced T1-weighted images known as "thin-rim enhancement" sign (Sakai et al. 1992) (Fig. 11.5). Signal intensity at the center of tuberculomas is low or slightly enhanced, but the signal intensity of the fibrotic rim is markedly enhanced. These MR findings correspond well to those of pathological specimens (Sakai et al. 1992; Kono et al. 1993; Kusumoto et al. 1994; Parmar et al. 2000; Chung et al. 2000; Schaefer et al. 2006). Therefore, when tuberculoma is suspected or attempts are made to distinguish it non-invasively from malignant nodules, pre- and post-contrast enhanced conventional MR imaging may be the most suitable procedure because tuberculoma is one of the most well-known diseases that show intense FDG uptake and is difficult to distinguish from malignant nodules by when FDG-PET or PET/CT is used (Chang et al. 2006).

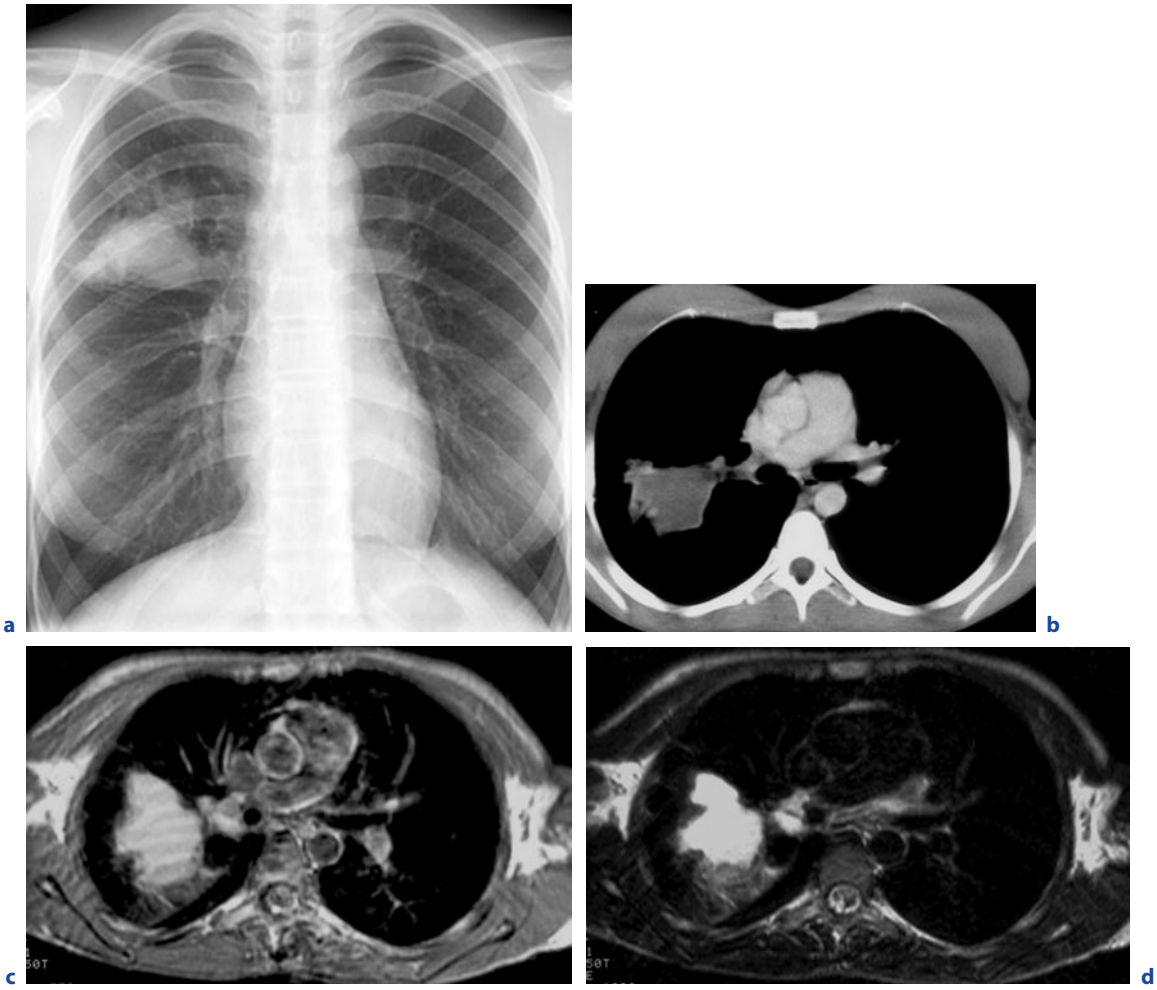

Fig. 11.4a–d. A 15-year-old female with bronchocele in the right upper lobe. Chest radiograph shows a mass in the right upper lung field (**a**). Contrast enhanced CT shows a mass with water density in the right upper lobe (**b**). Conventional T1-weighted SE (**c**) and T2-weighted turbo SE (**d**) images show the mass as high intensity due to mucus-filled bronchi and formation of a mucocele distal to the atelectatic segment, which was diagnosed as a bronchocele

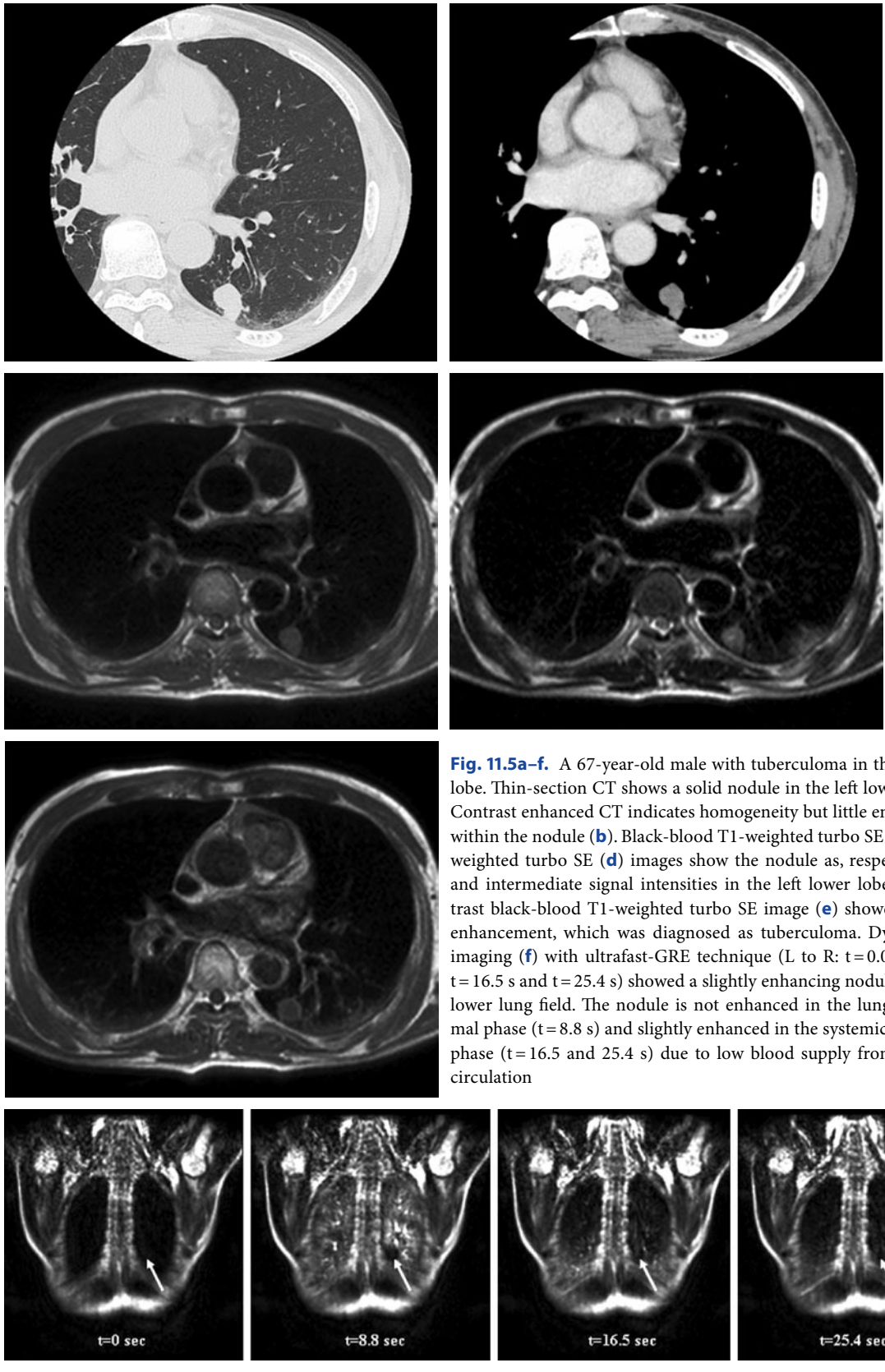

Fig. 11.5a–f. A 67-year-old male with tuberculoma in the left lower lobe. Thin-section CT shows a solid nodule in the left lower lobe (**a**). Contrast enhanced CT indicates homogeneity but little enhancement within the nodule (**b**). Black-blood T1-weighted turbo SE (**c**) and T2-weighted turbo SE (**d**) images show the nodule as, respectively, low and intermediate signal intensities in the left lower lobe. Post-contrast black-blood T1-weighted turbo SE image (**e**) showed thin-rim enhancement, which was diagnosed as tuberculoma. Dynamic MR imaging (**f**) with ultrafast-GRE technique (L to R: t = 0.0 s, t = 8.8 s, t = 16.5 s and t = 25.4 s) showed a slightly enhancing nodule in the left lower lung field. The nodule is not enhanced in the lung parenchymal phase (t = 8.8 s) and slightly enhanced in the systemic circulation phase (t = 16.5 and 25.4 s) due to low blood supply from bronchial circulation

11.3.1.3 Mucinous Bronchioalveolar Carcinoma

Adenocarcinoma of the lung constitutes a histologically and biologically heterogeneous group of tumors. Except for mucinous BAC, mucin production is seldom a truly prominent characteristic of this adenocarcinoma, so that there are no significant differences in the MR findings for adenocarcinoma of the lung and other subtypes of lung cancer. Mucinous BAC occasionally presents as a solitary pulmonary nodule with low or no uptake of contrast media on conventional post-contrast enhanced T1-weighted image, and thus may be difficult to differentiate from other benign nodules such as tuberculoma. However, many mucinous BACs demonstrate one of two radiological patterns, consolidation or diffuse disease. The consolidation may be segmental or may involve an entire lobe, and, with the exception of pulmonary vasculature, shows as high signal intensity on T2-weighted turbo SE images, which is known as "white lung sign" (Fig. 11.6). In addition, intratumoral vessels may be detected on contrast-enhanced T1-weighted images (Gaeta et al. 2000, 2001, 2002).

11.3.1.4 Hamartoma

Pulmonary hamartomas, the third most common cause of solitary pulmonary nodules, are considered benign neoplasms that originate in fibrous connective tissue beneath the mucus membrane of the bronchial wall (Bateson 1973; Siegelman et al. 1986). A few investigators have reported on MR imaging of hamartomas. Sakai et al. (1994) found that all hamartomas appeared as a signal of intermediate intensity on T1-weighted SE images and as one of high intensity on T2-weighted SE images and four out of six hamartomas had a lobulated appearance separated by septa on T1- or T2-weighted SE images. In addition, pulmonary hamartomas pathologically diagnosed as lipomatous hamartoma sometimes show with high signal intensity on T1-weighted SE and T2-weighted turbo SE images (Yilmaz et al. 2004). Therefore, when these radiological findings are associated with a pulmonary nodule the nodule can be suspected of being a hamartoma, and the enhancement pattern within the nodule should be evaluated on post-contrast enhanced T1-weighted SE images, where the regions with less enhancement correspond to core

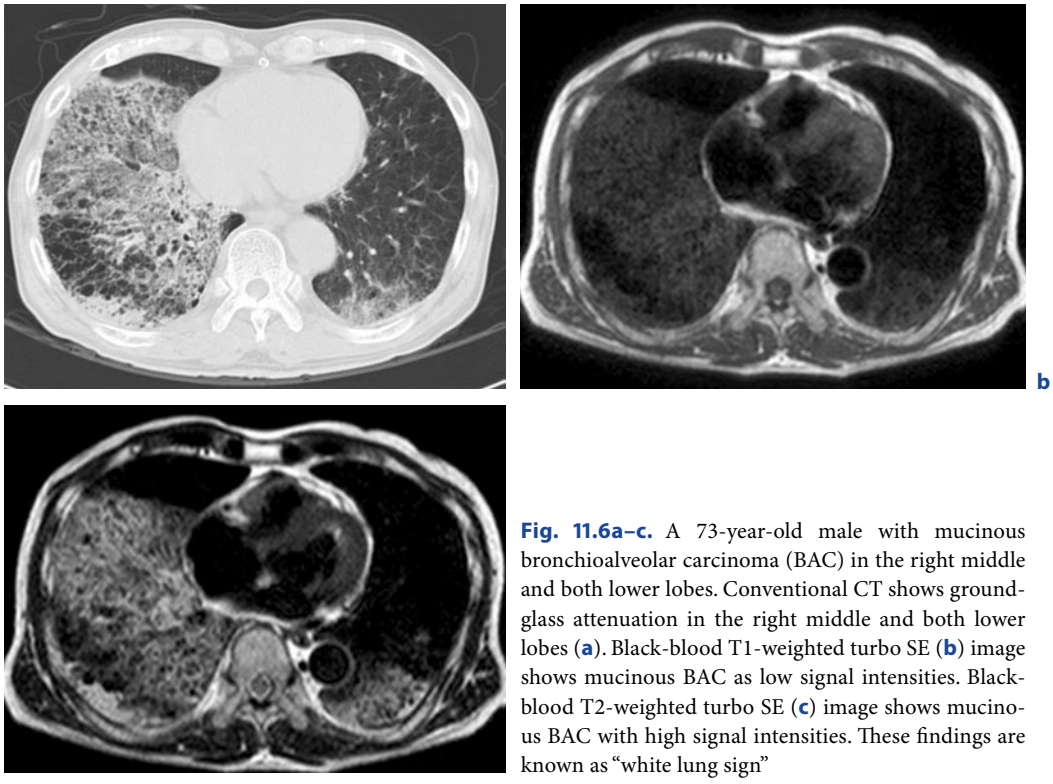

Fig. 11.6a–c. A 73-year-old male with mucinous bronchioalveolar carcinoma (BAC) in the right middle and both lower lobes. Conventional CT shows ground-glass attenuation in the right middle and both lower lobes (**a**). Black-blood T1-weighted turbo SE (**b**) image shows mucinous BAC as low signal intensities. Black-blood T2-weighted turbo SE (**c**) image shows mucinous BAC with high signal intensities. These findings are known as "white lung sign"

cartilaginous tissue and septa, and areas of marked contrast enhancement correspond to branching cleft-like mesenchymal connective tissue that dip into the cartilaginous core (Sakai et al. 1994) (Fig. 11.7).

11.3.1.5 Aspergilloma

Saprophytic aspergillosis (aspergilloma) is characterized by Aspergillus infection without tissue invasion. It typically leads to conglomeration of intertwined fungal hyphae admixed with mucus and cellular debris within a pre-existing pulmonary cavity or ectatic bronchus (Gefter 1992; Aquino et al. 1994). A typical radiological finding of aspergilloma is a solid, round or oval mass with soft-tissue opacity within a lung cavity. The mass is typically separated from the cavity wall by an airspace manifesting the so-called "air crescent" sign, and is often associated with thickening of the wall and adjacent pleura (Gefter 1992; Park et al. 2007). The most common underlying causes are healed tuberculosis, bronchiectasis, bronchial cyst and sarcoidosis. Other conditions that occasionally may be associated with aspergilloma include bronchogenic cyst, pulmonary sequestration, and pneumatoceles secondary to *Pneumocystis carinii* pneumonia in patients with acquired immunodeficiency syndrome.

The presence of a cavity within lung cancer is common and has been reported in 2%–16% of cases (Felson and Wiot 1977). In general, lung cancer with a cavity typically shows a cavity wall with a thickness of more than 4 mm, spiculate or irregular inner and outer margins, enlarged lymph nodes, and a soft-tissue

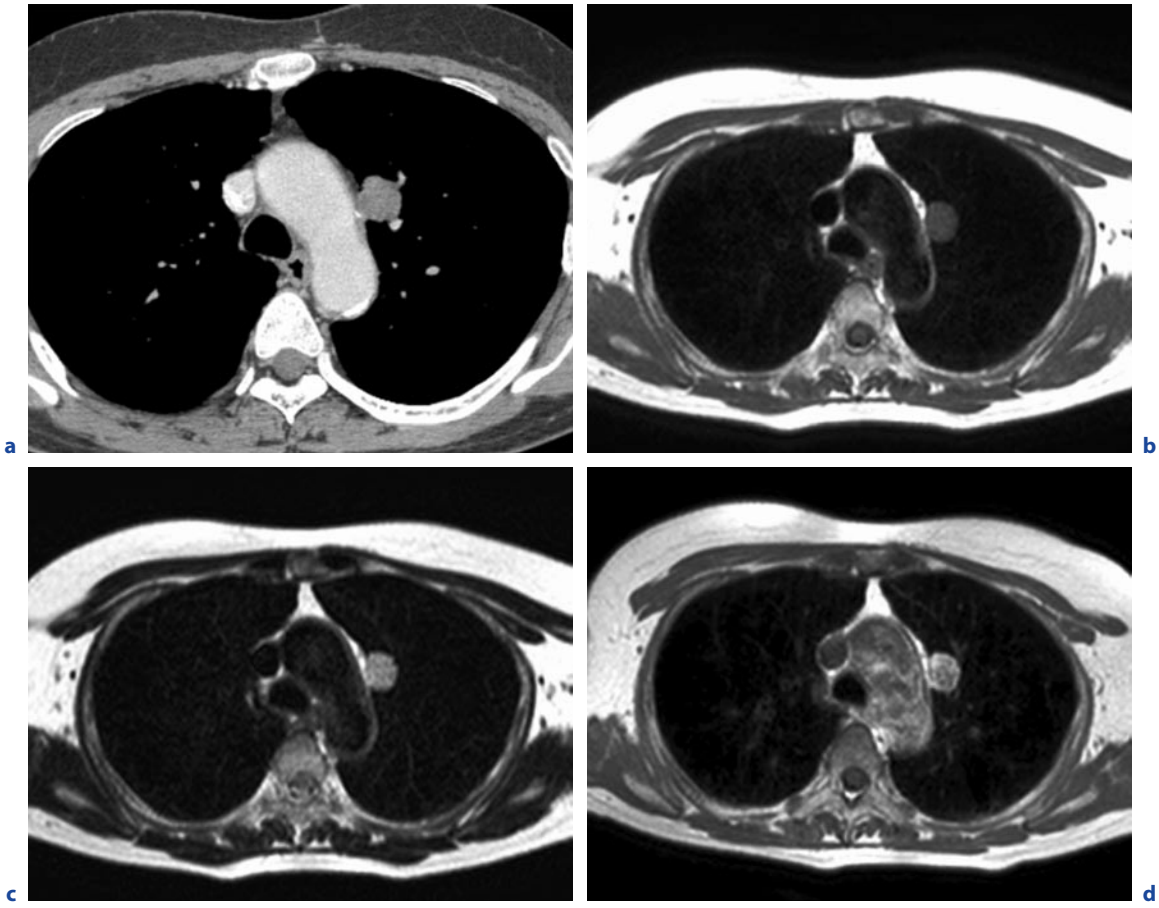

Fig. 11.7a–d. A 54-year-old male with hamartoma in the left upper lobe. Conventional contrast enhanced CT shows lobulated nodule in the left upper lobe (**a**). Black-blood T1-weighted turbo SE (**b**) and T2-weighted (**c**) images show a lobulated nodule as, respectively, low and high signal intensities in the left upper lobe. Post-contrast black-blood T1-weighted turbo SE (**d**) image shows less enhancement corresponding to core cartilaginous tissue, while areas of marked contrast enhancement correspond to cleft-like branching mesenchymal connective tissue

nodule or mass due to intracavitary tumorous mural regions associated with infiltration of the adjacent thoracic wall. In some cases, however, a lung cancer with a cavity may show a thin wall or "air crescent" sign on CXR or CT. It is therefore important to distinguish fungus ball from intracavitary tumorous mural regions by the "air crescent" sign in lung cancers with cavities, and pre- and post-contrast enhanced conventional T1- and T2-weighted SE or turbo SE images are helpful for this purpose.

Although a cavity may be present within lung cancer a viable lung cancer evidenced as a cavity and/or intracavitary mass shows a typical signal intensity pattern on pre- and post-contrast enhanced conventional T1- and T2-weighted SE or turbo SE images with as its characteristics a signal of low or intermediate intensity on pre-contrast enhanced T1-weighted images, one of intermediate or high intensity on T2-weighted images, and one of high intensity due to intensive and homogeneous enhancement on post-contrast enhanced

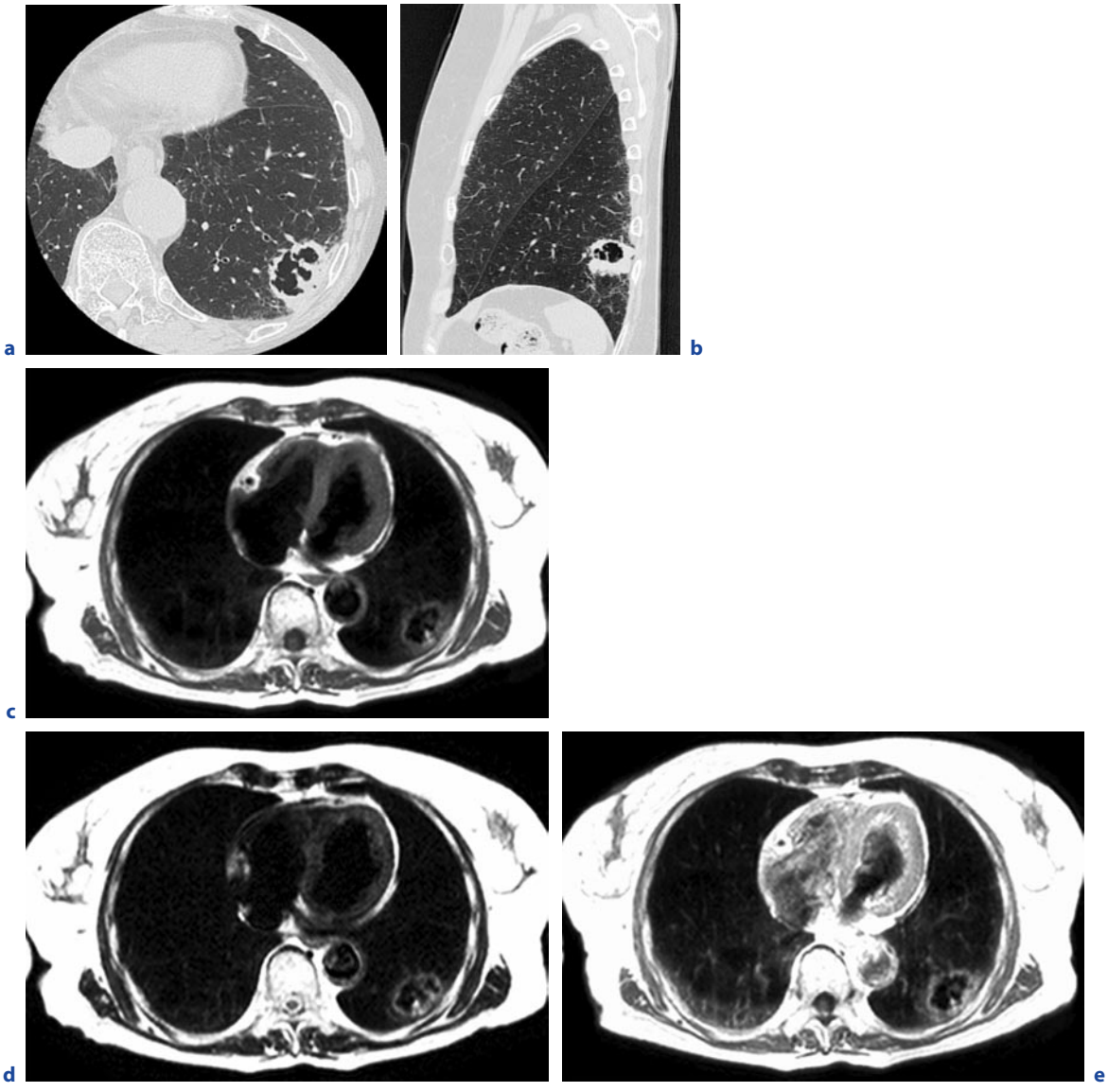

Fig. 11.8a–e. A 74-year-old male with squamous cell carcinoma in the left lower lobe. Thin-section CT (**a**) and sagittal reformat (**b**) show mass with irregularly thickened cavity wall in the left lower lobe. Black-blood T1-weighted turbo SE (**c**) and T2-weighted (**d**) images show mass with irregularly thickened cavity wall as, respectively, low and high signal intensities in the left lower lobe. Post-contrast black-blood T1-weighted turbo SE (**e**) image shows well-enhanced cavity wall corresponding to lung cancer

T1-weighted images (Ma et al. 1985; van der Heide et al. 1985; Zinreich et al. 1988; Herold et al. 1989; Fujimoto et al. 1994; Blum et al. 1994) (Fig. 11.8). In aspergilloma cases, on the other hand, the signal intensity of the intracavitary lesion is especially reduced on the T2-weighted SE or turbo SE image because of the presence of calcium, air, or ferromagnetic elements resulting from Aspergillus infection (Herold et al. 1989; Fujimoto et al. 1994; Blum et al. 1994) (Fig. 11.9). Because of the presence of the ferromagnetic elements of iron, magnesium, and manganese are essential to the metabolism of amino acids by fungi, Fujimoto et al. (1994) have suggested that the reduction in signal intensity on T1-weighted images and the marked reduction on T2-weighted images are characteristics of aspergilloma as well as mycetomas, and may be useful for differentiation of aspergilloma from intracavitary tumorous mural nodules.

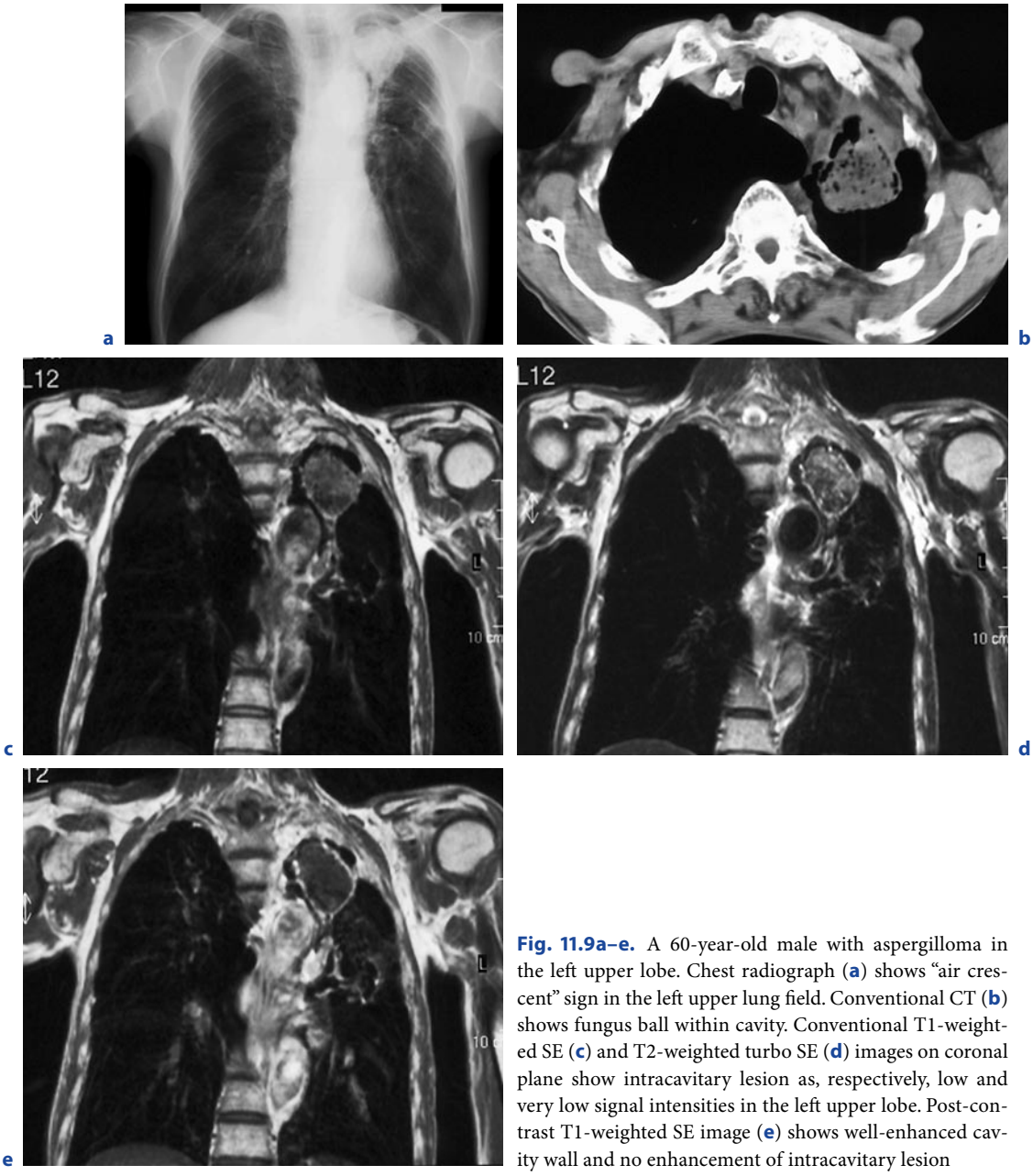

Fig. 11.9a–e. A 60-year-old male with aspergilloma in the left upper lobe. Chest radiograph (**a**) shows "air crescent" sign in the left upper lung field. Conventional CT (**b**) shows fungus ball within cavity. Conventional T1-weighted SE (**c**) and T2-weighted turbo SE (**d**) images on coronal plane show intracavitary lesion as, respectively, low and very low signal intensities in the left upper lobe. Post-contrast T1-weighted SE image (**e**) shows well-enhanced cavity wall and no enhancement of intracavitary lesion

11.3.2 Dynamic Contrast-enhanced MR Imaging of Pulmonary Nodules

Although in some cases benign or malignant focal lesions can be differentiated from others by using pre- and post-contrast enhanced conventional T1- or T2-weighted SE or turbo SE imaging, significant overlaps have been observed between benign and malignant lesions in routine clinical practice (Kono et al. 1993; Kusumoto et al. 1994). To overcome this problem, dynamic contrast-enhanced MR imaging has been proposed as an alternative technique for diagnosis and/or management of pulmonary nodules (Table 11.1). As a result of advances in MR systems and pulse sequences, there are now three major methods for dynamic MR imaging of the lung. Many investigators have proposed dynamic MR imaging be used for two-dimensional (2D) SE or turbo SE sequences or for various types of 2D or three-dimensional (3D) gradient-echo (GRE) sequences and that enhancement patterns within nodules and/or parameters determined from signal intensity-time course curves be assessed visually. These curves represent first transit and/or recirculation and wash-out of contrast media in 5 min or more with repeated breath holding (Kono et al. 1993; Kusumoto et al. 1994; Hittmair et al. 1995; Gückel et al. 1996; Ohno et al. 2002, 2004a; Fujimoto et al. 2003; Schaefer et al. 2004, 2006; Kono et al. 2007; Donmez et al. 2007). Taking into account the inherent inhomogeneous composition of many intraindividual lung cancers and even within benign lesions such as central necrosis, only a dynamic contrast-enhanced 3D approach has the chance of depicting all underlying histologies. This is important for the primary diagnosis as well as during follow up examinations to assure evaluation of the same region of interest again. Recently, dynamic contrast enhanced MR perfusion imaging has been proposed for quantitative and qualitative assessment of regional pulmonary perfusion abnormalities by using 2D or 3D ultra-fast GRE sequences with sharp bolus profiles (Hatabu et al. 1996, 1999; Amundsen et al. 1997, 2000; Levin et al. 2001; Matsuoka et al. 2001; Ohno et al. 2002, 2004c, 2005, 2007a, b; Fink et al. 2004). This technique allows for directly assessing the first passage of contrast media within nodules in less than 35 s within a single breath hold and to evaluate blood supply to nodules from pulmonary and/or bronchial circulation (Ohno et al. 2002, 2004c). It should be noted though that the ideal acquisition of contrast enhanced dynamic studies of tumor perfusion should not be limited to the first pulmonary passage of the contrast agent. Tumors will be supplied by systemic, bronchial arteries instead of pulmonary arteries. In this case or due to inherent slow blood flow within a tumor an examination in a single breath hold might not be sufficient in detecting the full perfusion cycle of wash-in and wash-out. Examination of prolonged wash-out always reveals an underlying reperfusion of pulmonary tissue by both pulmonary and bronchial arteries. This circumstance has not been accounted for in the usual models for quantification of tissue perfusion so far.

Although there are various dynamic MR techniques, reported sensitivities range from 94% to 100%, specificities from 70% to 96%, and accuracies of more than 94% (Kono et al. 1993, 2007; Kusumoto et al. 1994; Hittmair et al. 1995; Gückel et al. 1996; Ohno et al. 2002, 2004a; Fujimoto et al. 2003; Schaefer et al. 2004, 2006; Donmez et al. 2007). These specificities and accuracies for dynamic MR imaging are superior to those reported for dynamic CT, and almost equal to or superior to those for FDG-PET or PET/CT (Swensen et al. 1992, 1996, 2000; Dewan et al. 1993; Kono et al. 1993; Patz et al. 1993; Kusumoto et al. 1994; Hittmair et al. 1995; Yamashita et al. 1995; Bury et al. 1996; Gückel et al. 1996; Zhang and Kono 1997; Ohno et al. 2002, 2004a; Fujimoto et al. 2003; Herder et al. 2004; Schaefer et al. 2004, 2006; Yi et al. 2004, 2006; Jeong et al. 2005; Joshi et al. 2005; Mori et al. 2005; Bryant and Cerfolio 2006; Christensen et al. 2006; Donmez et al. 2007; Kim et al. 2007; Kono et al. 2007; Lee et al. 2007). Therefore, dynamic contrast-enhanced MR imaging may perform a complementary role in the diagnosis of pulmonary nodules assessed with FDG-PET or PET/CT. Although these results are highly promising further research in this field may be necessary in the light of recently published data regarding the MR signal dependency in perfusion studies on the contrast agent concentration. As quantification of perfusion parameters is dependent on an almost linear relationship of signal to concentration great care has to be taken regarding the dosage and application of contrast agents (Puderbach et al. 2008).

Although differentiation of malignant from benign pulmonary nodules by means of dynamic MDCT, dynamic MRI and PET or PET/CT with FDG has been tried in several studies, accurate separation of active infectious nodules from malignant neoplasms on the basis of dynamic CT and MR parameters and uptakes of FDG can be extremely difficult in view of the underlying pharmacokinetical, pathological and biological properties of malignant neoplasms and active infectious nodules. In addition, when considering the management of pulmonary nodules in clinical practice, it may be helpful to differentiate pulmonary nodules requiring further intervention and treatment (low or high grade

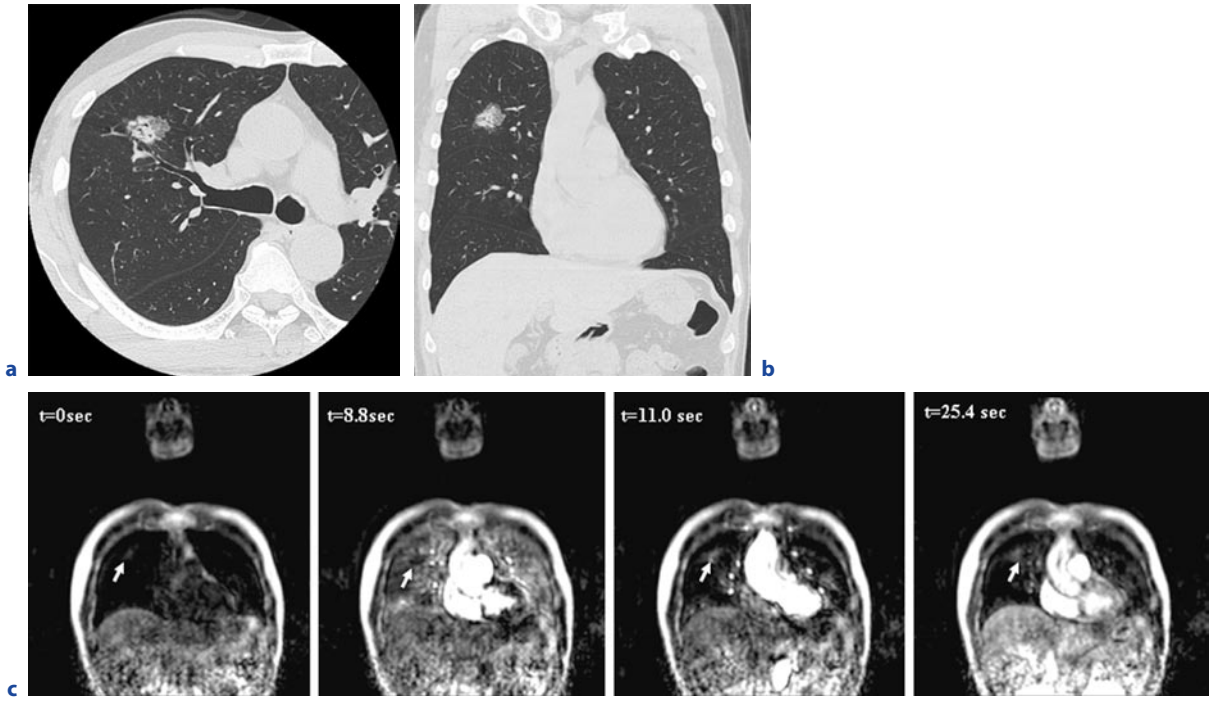

Fig. 11.10a–c. A 57-year-old female with adenocarcinoma with mixed subtype. Thin-section CT (**a**) and coronal reformat (**b**) show partly solid nodule in the right upper lobe. Dynamic MR imaging (**c**) with ultra-fast GRE technique (L to R: t = 0.0 s, t = 8.8 s, t = 11.0 s and t = 25.4 s) shows well-enhanced nodule (*arrow*) in the right upper lung field. The nodule was not enhanced in the lung parenchymal phase (t = 8.8 s) and well enhanced in the systemic circulation phase (t = 11.0 and 25.4 s) due to enhanced blood supply from bronchial circulation

malignant tumors and active infectious nodules) from pulmonary nodules requiring no further evaluation (benign tumors and chronic infectious nodules) rather than to differentiate between malignant nodules and other nodules. For this latter differentiation, ultra-fast dynamic MR imaging can divide all nodules into the two categories (Figs. 11.5 and 11.10) (Ohno et al. 2002). This means that it may be better to use dynamic MR imaging in a complementary role to CT and FDG-PET or PET/CT to determine whether further intervention and treatment are indicated rather than to differentiate pulmonary nodules into malignant nodules and other nodules in routine clinical practice.

On the other hand, the results of several comparative studies of findings obtained with dynamic MR parameters and with immuno-histopathological examination of small peripheral lung cancers, the former showed good correlation with tumor angiogenesis (Fujimoto et al. 2003; Schaefer et al. 2006), and the potential for more accurate differentiation of subtypes of small peripheral adenocarcinomas than is possible with thin-section CT, or for prognosis both before and after treatment (Fujimoto et al. 2003; Ohno et al. 2005; Schaefer et al. 2006).

Moreover, ultra-fast 3D dynamic MR data can also be used for the prediction of postoperative lung function for non-small cell lung cancer patients (Ohno et al. 2004b, 2007b). The semi-quantitative regional perfusion obtained from ultra-fast dynamic MR imaging shows good correlation with that assessed by perfusion scintigraphy, with a reported limit of agreement of ±6%, which is insignificant enough to make ultra-fast dynamic MR imaging suitable for clinical purposes (Ohno et al. 2004b). Moreover, the prediction of postoperative lung function derived from dynamic MR imaging was more accurate than that derived from perfusion scintigraphy, single photon emission tomography (SPECT) or qualitatively assessed MDCT, which is predicted postoperative lung function from preoperative lung function and the number of lung segments in the total and resected lung evaluated by pulmonary surgeons, and the predictive accuracy is almost equal to that obtained with quantitatively assessed MDCT based on density-masked CT technique (Ohno et al.

Table 11.2. Stage grouping of lung cancer

Overall stage	T stage	N stage	M stage
Occult carcinoma	Tx	N0	M0
Stage 0	Tis (in situ)	N0	M0
Stage IA	T1	N0	M0
Stage IB	T2	N0	M0
Stage IIA	T1	N1	M0
Stage IIB	T2	N1	M0
	T3	N0	M0
Stage IIIA	T1or T2	N2	M0
	T3	N1or N2	M0
Stage IIIB	Any T	N3	M0
	T4	Any N	M0
Stage IV	Any T	Any N	M1

Table 11.3. T classification – primary tumor

TX	Primary tumor cannot be assessed, or tumor proven by the presence of malignant cells in sputum or bronchial washings but not visualized by imaging or bronchoscopy
T0	No evidence of primary tumor
Tis	Carcinoma in situ
T1	Tumor 3 cm or less in greatest dimension, surrounded by lung or visceral pleura, without bronchoscopic evidence of invasion more proximal than the lobar bronchus (i.e., not in the main bronchus)[a]
T2	Tumor with any of the following features of size or extent
	× More than 3 cm in greatest dimension
	× Involves main bronchus, 2 cm or more distal to the carina
	× Invades visceral pleura
	× Associated with atelectasis or obstructive pneumonitis that extends to the hilar region but does not involve the entire lung
T3	Tumor of any size that directly invades any of the following: chest wall (including superior sulcus tumors), diaphragm, mediastinal pleura, parietal pericardium; or tumor in the main bronchus less than 2 cm distal to the carina but with involvement of the carina; or associated atelectasis or obstructive pneumonitis of the entire lung
T4	Tumor of any size that invades any of the following: mediastinum, heart, great vessels, trachea, esophagus , vertebra body, carina; separate tumor nodule(s) in the same lobe; tumor with malignant pleural effusion[b]

[a]The uncommon superficially spreading tumor of any size with its invasive component limited to the bronchial wall, which may extend proximal to the main bronchus, is classified as T1

[b]Most pleural effusions associated with lung cancer are due to tumor. In a few patients, however, multiple cytopathological examinations of pleural fluid are negative for tumor, and the fluid is non-bloody and is not an exudate. Where these elements and clinical judgment dictate that the effusion is not related to the tumor, the effusion should be excluded as a staging element and the patient should be classified as T1, T2 or T3

Table 11.4. N classification – regional lymph nodes

NX	Regional lymph nodes cannot be assessed
N0	No regional lymph node metastasis
N1	Metastasis in ipsilateral peribronchial and/or ipsilateral hilar lymph nodes and intrapulmonary lymph nodes, including involvement by direct extension
N2	Metastasis in ipsilateral mediastinal, and/or subcarinal lymph node(s)
N3	Metastasis in contralateral mediastinal, contralateral hilar, ipsilateral or contralateral scalene, or supraclavicular lymph node(s)

Table 11.5. M classification – distant metastasis

MX	Distant metastasis cannot be assessed
M0	No distant metastasis
M1	Distant metastasis includes separate tumor nodule(s) in a different lobe (ipsilateral or contralateral)

2007b). Dynamic MR imaging may therefore be useful not only for the characterization of pulmonary nodules, but prediction of postoperative lung function may also assist the management of pulmonary nodules, including determination of whether further intervention and treatment and/or operability are indicated for lung cancer patients.

11.4 Assessment of TNM Stages

The international TNM classification proposed by the International Union against Cancer (UICC) has been widely used in the investigation and treatment of lung cancer (Tables 11.2–11.5), and shows that survival rates have improved with more accurate staging and more accurate differentiation between those patients who are candidates for surgical resection and those who are judged to be inoperable but would benefit from chemotherapy, radiotherapy, or both (Sobin and Wittekind 2002). Therefore, accurate radiological staging may affect the management as well as the prognosis of patients. However, only approximately one-half of the TNM stages determined with CT systems in the past have agreed with operative staging, with patients being both under- and over-staged (Lewis et al. 1990; Gdeedo et al. 1997).

Currently, newly developed MDCT systems, FDG-PET or PET/CT, are considered useful for precise assessment of tumor extent because of their multiplanar capability and for accurate diagnosis of metastatic lymph nodes by analyzing the glucose metabolism of cancer cells in lung cancer patients. However, since 1991 it has been suggested that MR imaging, with its multiplanar capability and better contrast resolution of tumor and mediastinum or of tumor and chest wall or both than that of CT, may also be useful, but only for the assessment of mediastinal and chest wall invasions and determination of the short axis diameter of certain mediastinal lymph nodes (Webb et al. 1991). However, recent advancements in MR systems, improved or newly developed pulse sequences and/or utilization of contrast media has resulted in improved diagnosis of TNM staging for lung cancer patients (Table 11.6).

11.4.1 MR Assessment of T Classification

T classification is the descriptor given to the primary tumor and its local extent (Sobin and Wittekind 2002). The definitions are given in Table 11.3. While the T factor is subdivided into four groups, the distinction between T3 and T4 tumors is critical because it represents the dividing line between conventional surgical and non-surgical management for NSCLC patients (Armstrong 2000). It is therefore more important to distinguish T3 from T4 tumors than to differentiate T1 and T2 tumors and determine nodal staging. For this reason, MR imaging may be helpful for assessment of mediastinal invasion, chest wall invasion and distinguishing primary tumors from secondary changes such as atelectasis or obstructive pneumonia, although it may be difficult to distinguish simple extension of the tumor into the mediastinal pleura or pericardium (T3) from actual invasion (T4).

Table 11.6. Recommended MR protocol for lung cancer staging

No.	Recommended sequence	TR (ms)	TE (ms)	FA (°)	Matrix	Respiration	Suggestion
1	Pre-contrast-enhanced ECG-gated T1W-SE or TSE	1 <R-R>	15–25	N/A	256×256	RT or RG	
2	ECG- and respiratory-gated T2W-TSE	2 or 3 <R-R>	90–100	N/A	256×256	RT or RG	ETL should be less than 15
3	Respiratory-gated STIR TSE	Up to respiratory cycle	15	N/A	256×256	RG	ETL should be less than 5, if sequentially-reordered phase encoding scheme is used
4	ECG-gated contrast-enhanced MR angiography	5.7	1.9	20	256×128–256	BH	k-space segmentation should be adapted
	Time-resolved contrast-enhanced MR angiography	4.0	1.2	20–30	512×333	BH	Temporal resolution should be less than 4 s
5	Post contrast-enhanced ECG-gated T1W-SE or TSE	1 <R-R>	15–25	N/A	256×256	RT or RG	

SE: spin-echo, TSE: turbo spin-echo, GRE: gradient echo, TR: repetition time, TE: echo time, FA: flip angle, RT: respiratory-trigger, RG: respiratory-gated, ETL: echo train length

11.4.1.1 Mediastinal Invasion

Many surgeons consider minimal invasion of mediastinal fat as resectable (Quint and Francis 1999), so that clinicians want to know whether minimal mediastinal invasion (T3 disease) or actual invasion (T4 disease) has occurred before considering surgical resection. The accuracy of CT for evaluating hilar and mediastinal invasion of lung cancer has been investigated extensively over the last two decades. Sensitivity for assessment of mediastinal invasion by single detector computed tomography with or without the use of helical scanning ranged from 40% to 84% and specificity from 57% to 94% (Baron et al. 1982; Martini et al. 1985; Quint et al. 1987, 1995; Rendina et al. 1987; Glazer et al. 1989; Herman et al. 1994; White et al. 1994; Takahashi et al. 1997).

The RDOG study compared CT with MR imaging for 170 patients with non-small cell lung cancer, although only T1-weighted images obtained without the use of cardiac or respiratory gating techniques were assessed in this study (Webb et al. 1991). Although there was no significant difference between the sensitivity (63% and 56% for CT and MR imaging, respectively) and the specificity (84% and 80%) for distinguishing between T3-T4 tumors and T1-T2 tumors in this study, the RDOG reported that 11 patients showed mediastinal invasion and that the superior contrast resolution of MR imaging conferred a slight but statistically significant advantage over CT for accurate diagnosis of mediastinal invasion. In addition, delineation of tumor invasion of pericardium (T3) or heart (T4) was superior on MR imaging compared with CT scan when the cardiac-gated T1-weighted sequence was used for improved avoidance of cardiac motion artifacts (White 1996). The normal pericardium has low signal intensity. Direct invasion of the cardiac chambers is readily demonstrated on T1-weighted images, because blood flowing through the cardiac chambers is signal void, so that the tumor is conspicuous because of its higher signal intensity. However, the accuracy of minimal mediastinal invasion assessment by both CT scanning and MR imaging is limited because it depends on visualization of the tumor within the mediastinal fat (Wong et al. 1999). In contrast to the assessment of mediastinal invasion, Mayr et al. (1987) found CT scanning to be more accurate than MR imaging in visualizing and assessing both normal and abnormal airways. They evaluated 319 normal and 79 abnormal bronchoscopically visualized bronchi. Their study found that CT scanning was accu-

rate in all cases, whereas MR imaging correctly identified only 45% of normal bronchi and 72% of abnormal bronchi (Magdeleinat et al. 2001). This discrepancy can be attributed both to the higher spatial resolution of CT scanning and to the low intrinsic MR imaging signal of air. Therefore, the relationship of lung cancer to central endobronchial extension is more accurately demonstrated on CT scans.

Recent advancement in MR systems, improved pulse sequences and utilization of contrast media have resulted in the introduction of new MR imaging techniques for assessment of mediastinal invasion of lung cancer. Contrast-enhanced MR angiography has been used for assessment of cardiovascular or mediastinal invasions (Takahashi K et al. 2000; Ohno et al. 2001). Ohno et al. (2001) described a series of 50 NSCLC patients with suspected mediastinal and hilar invasion of lung cancer visualized with contrast-enhanced CT scans, cardiac-gated MR imaging, and non-cardiac- and cardiac-gated contrast-enhanced MR angiographies (Fig. 11.11). In this study, sensitivities, specificities and accuracies of both contrast-enhanced MR angiography ranged from 78% to 90%, 73% to 87%, and 75% to 88%, respectively. These values were higher than those of contrast-enhanced single helical CT and conventional T1-weighted imaging (Ohno et al. 2001). Thus, contrast-enhanced MR angiography is thought to improve the diagnostic capability of MR imaging for mediastinal and hilar invasion.

In 2005, another new technique, cine MR imaging obtained with a steady-state free precession (SSFP) sequence was introduced as useful for evaluation of cardiovascular invasion in patients with thoracic mass (Seo et al. 2005). In this study, as well as previous electron beam CT or traditional cine MR studies (Murata et al. 1994; Sakai et al. 1997), the assessment of sliding

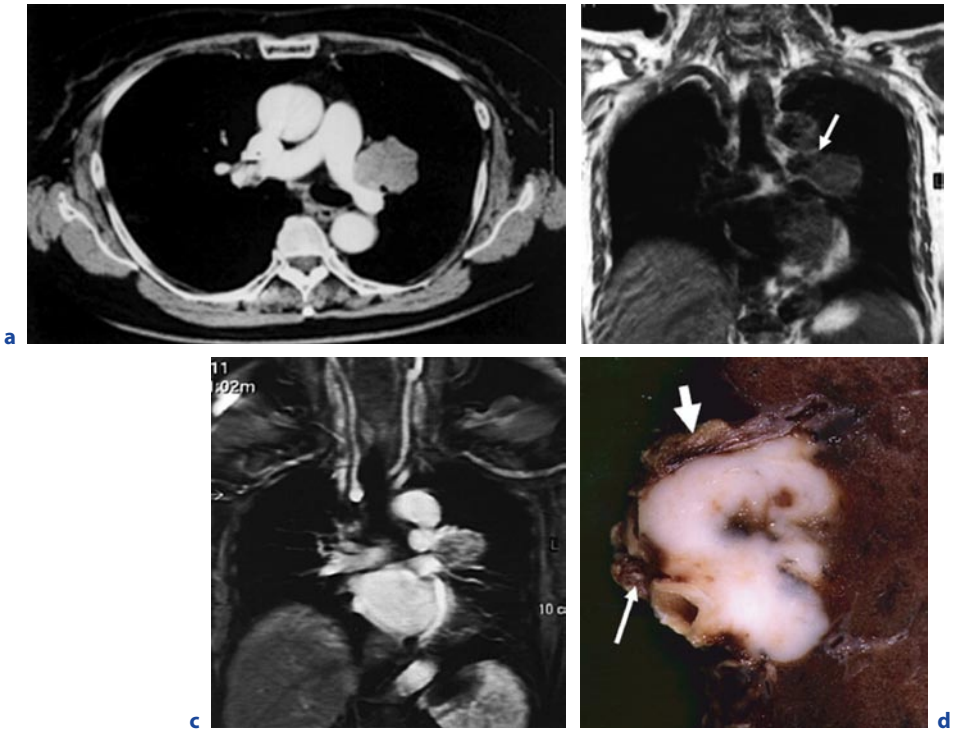

Fig. 11.11a–d. A 68-year-old female with squamous cell carcinoma in the left upper lobe. Contrast enhanced thin-section CT (**a**) suggests invasion to pulmonary vein and mediastinum, while conventional T1-weighted image (**b**) on coronal plane suggests invasion to pulmonary artery and mediastinum (*arrow*). Contrast-enhanced MR angiography (**c**) clearly shows invasion to pulmonary artery and vein, but not mediastinal invasion due to visualization of mediastinal fat between pulmonary artery and pulmonary vein as a *black area*. Macroscopical finding of the resected left upper lobe (**d**) shows invasion to left pulmonary artery (*arrow*) and left superior pulmonary vein (*large arrow*), but not mediastinal invasion

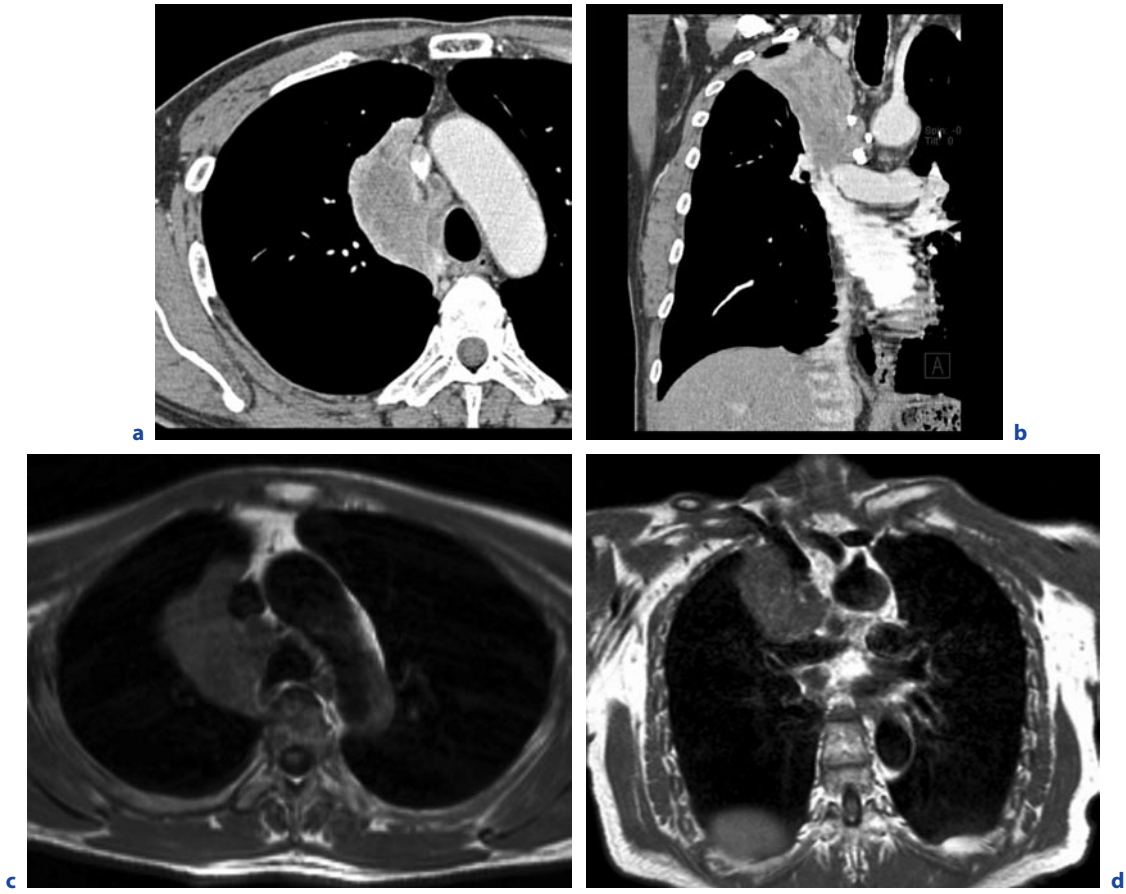

Fig. 11.12a–d. A 61-year-old male with squamous cell carcinoma in the right upper lobe. Contrast enhanced CT (**a**) suggests mediastinal invasion, while contrast enhanced coronal reformat (**b**) clearly demonstrates mediastinal invasion. Black-blood T1-weighted images on axial (**c**) and coronal (**d**) planes also clearly demonstrate invasion to superior venous cava and mediastinum

motions between thoracic masses and adjacent mediastinal structure demonstrated a very high diagnostic capability (sensitivity: 100%, specificity: 92.9%, accuracy: 94.4%) (Seo et al. 2005). However, only 9 of 26 lung cancer patients were included in this study since the others had mediastinal tumors. Further investigation thus seems to be warranted to determine the actual diagnostic capability of cine MR imaging for mediastinal invasion in NSCLC patients.

In addition, MDCT has been widely utilized during the past five years or so for routine clinical practice, and it was found that thin-section multiplanar reformatted (MPR) imaging from thin-section volumetric MDCT data was useful for the evaluation of *T classification* due to its multiplanar capability (Higashino et al. 2005). Higashino et al. (2005) suggested that mediastinal invasion that can be assessed from thin-section coronal MPR images with 1 mm section thickness with greater sensitivity, specificity and accuracy than can be achieved with routine MDCT with 5 mm section thickness, and with slightly better specificity and accuracy than with thin-section axial MDCT with 1 mm section thickness. Although MR imaging is considered to show superior tissue contrast to that of MDCT, the similar multiplanar capability, faster scan time and better spatial resolution of thin-section MDCT may result in better assessment of mediastinal invasion in NSCLC patients than by previously described MR techniques (Fig. 11.12). Further investigations as well as comparative studies of thin-section MDCT and previously described or newly developed MR imaging techniques thus seem to be warranted to determine the actual significance of MR imaging for assessment of mediastinal invasion in routine clinical practice.

11.4.1.2 Distinguishing Lung Cancer from Secondary Change

Distinguishing primary lung cancer from secondary change is important for assessment of tumor extent and the therapeutic effect of chemotherapy and/or radiotherapy. While the therapeutic effect of conservative therapy has been assessed by using World Health Organization (WHO) criteria or response evaluation criteria in solid tumors (RECIST) (World Health Organization 1979; Therasse et al. 2000), it would be difficult to use CXR or plain or contrast-enhanced CT to evaluate tumor extent or therapeutic effect for cases with atelectasis or obstructive pneumonia.

MR imaging, on the other hand, has potential for distinguishing lung cancer from secondary change due to atelectasis or pneumonitis (Kono et al. 1993). In some cases, it can be difficult to distinguish lung cancer from post-obstructive atelectasis or pneumonitis because these secondary changes tend to be enhanced to a similar degree as the central tumor on contrast-enhanced CT scan. On T2-weighted MR imaging, however, post-obstructive atelectasis and pneumonitis often show higher signal intensity than does the central tumor. Bourgounin et al. (1991) evaluated the histological findings of obstructive pneumonitis or atelectasis in patients who had undergone surgical resection of lung cancer and had been evaluated preoperatively with MR imaging. They found that cholesterol pneumonitis and mucus plugs displayed higher signal intensity than the tumor on T2-weighted images, while atelectasis and organizing pneumonitis were isointense to the tumor. Kono et al. (1993) described a series of 27 patients with central lung cancer associated with atelectasis or obstructive pneumonitis (Fig. 11.13). These patients were examined with post-contrast enhanced T1-weighted MR imaging and the central tumor could be differentiated from adjacent lung parenchymal disease in 23 out of 27 patients (85%). The tumor was of lower signal intensity than the adjacent lung disease in 18 cases (67%) and of higher signal intensity in 5 (18%). These differences in signal intensity between primary tumor and secondary change were considered to be due to the presence of invasion of pulmonary vasculatures. Therefore, the use of T2-weighted or post-contrast enhanced T1-weighted images for assessment of tumor size and secondary change may be helpful for precise evaluation of tumor extent at the initial staging and for accurate prognosis for patients and assessment of therapeutic effect after conservative therapy and/or for comparative studies of standard and new chemo- and/or radiotherapy regimens (Ohno et al. 2000).

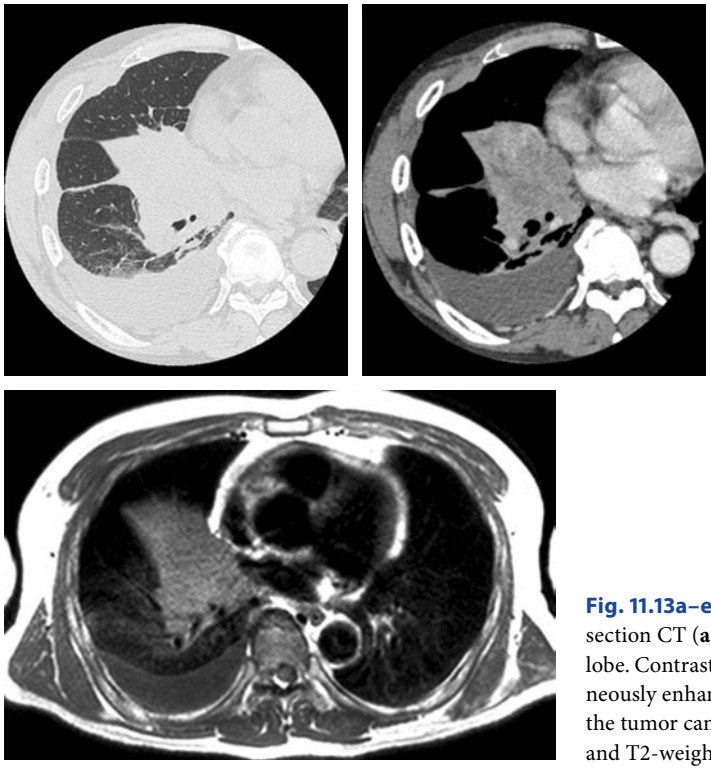

Fig. 11.13a–e. A 59-year-old male with adenocarcinoma. Thin-section CT (**a**) shows atelectasis in the right middle and lower lobe. Contrast enhanced thin-section CT (**b**) shows homogeneously enhanced ateletasis and pleural effusion, but the extentof the tumor cannot be determined. Black-blood T1-weighted (**c**) and T2-weighted (**d**) *see next page*

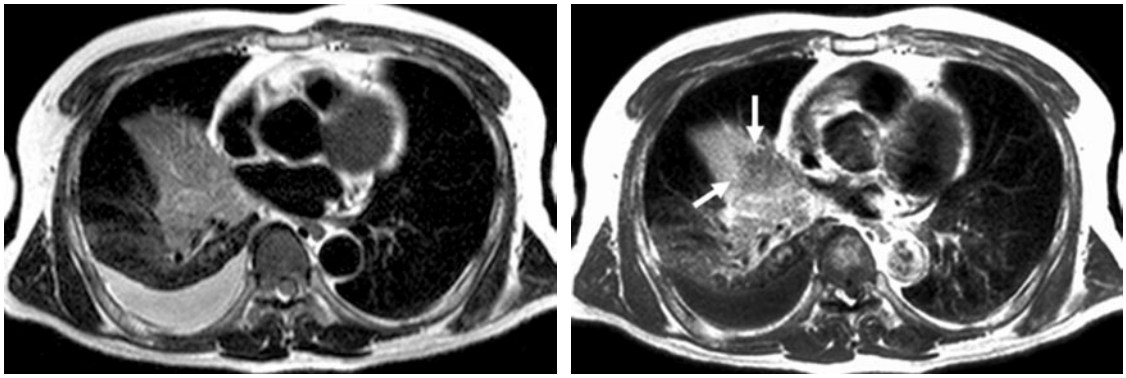

d e

Fig. 11.13a–e. *(continued)* images show atelectasis and the tumor as, respectively, low and intermediate signal intensity. Mediastinal invasion is suspected,while pleural effusion is clearly seen. Post-contrast black-blood T1-weighted image (**e**) clearly shows the extent of lung cancer and secondary change *(arrow)*

11.4.1.3 Chest Wall Invasion

Chest wall invasion used to be considered a contraindication for surgical excision of lung cancer, but recent surgical advances have made chest wall excision feasible for the treatment of locally aggressive lung cancer and giving patients a better chance of survival (Magdeleinat et al. 2001). Preoperative visualization of chest wall invasion may therefore be helpful for surgical planning. On conventional CT scan, rib destruction is the only reliable sign of chest wall invasion since soft tissue masses in the chest wall correlate statistically with chest wall invasion. However, they are not reliable indicators for an individual patient, so that focal chest pain may still be the most reliable indicator of chest wall invasion. In fact, the reliability of conventional CT assessment of chest wall invasion in lung cancer patients varies widely with reported sensitivities ranging from 38% to 87% and specificities from 40% to 90% (Quint and Francis 1999). In addition to the technique of inducing artificial pneumothorax described elsewhere (Watanabe et al. 1991; Yokoi et al. 1991), Murata et al. (1994) reported that dynamic expiratory multi-section CT reviewed as a cine loop was 100% accurate for identification of both chest wall and mediastinal invasion.

Another study has suggested that ultrasound (US) is an effective technique for diagnosis of chest wall invasion (Suzuki et al. 1993). In this study, 120 lung cancer patients were examined, in 19 of whom invasion was pathologically proved. Sensitivity, specificity and accuracy of US were 100%, 98%, and 98%, respectively, while the corresponding values for conventional CT used in the same study were only 68%, 66%, and 67% (Suzuki et al. 1993). Therefore, US is also considered useful for assessment of chest wall invasion by some chest physicians, although the diagnostic capability of US depends on the experience and technical capability of the clinician.

Because of its multiplanar capability and better tissue contrast resolution compared to CT, MR imaging has also been advocated as effective for assessment of chest wall invasion (Rapoport et al. 1988; Heelan et al. 1989; Webb et al. 1991; Padovani et al. 1993; Bonomo et al. 1996). Sagittal and coronal plane images are better than axial CT images for displaying the anatomical relationship between tumor and chest wall structures (Bonomo et al. 1996; Freundlich et al. 1996). MR imaging shows infiltration or disruption of the normal extra pleural fat plane on T1-weighted images or parietal pleural signal hyper intensity on T2-weighted images (Fig. 11.14). In addition, when STIR turbo SE imaging is used for this purpose, it can demonstrate lung cancer as high signal intensity within the suppressed signal intensities of chest wall structures, enabling clinicians to easily determine the tumor extent within chest wall (Fig. 11.14c). Moreover, Padovani et al. (1993) have suggested that the diagnostic yield can be further improved by intravenous administration of contrast media. In addition, superior sulcus or Pancoast tumors are good candidates for the demonstration of chest wall invasion on MR imaging. Since superior sulcus tumors occur in close proximity to the lung apex, their imaging has to include an evaluation of the relationship between the tumor and the brachial plexus, subclavian artery and vein, and adjacent chest wall. The axial scan plane of a CT scan is suboptimal for examining the lung apex where superior sulcus tumors are located, while direct

a

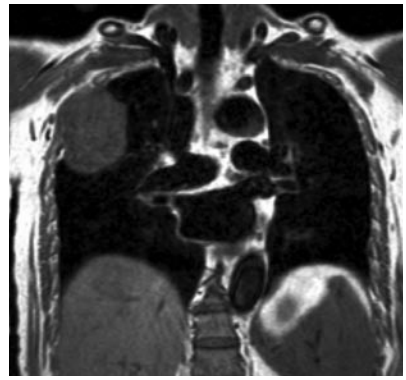

b

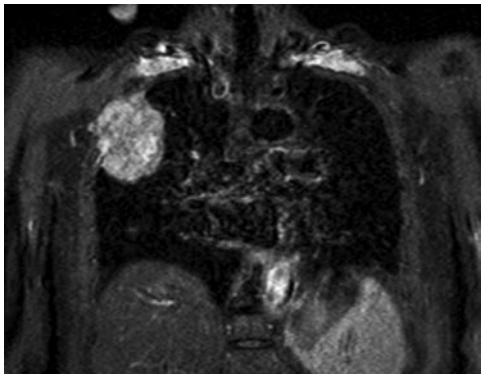

c

Fig. 11.14a–c. A 71-year-old male with adenocarcinoma in the right upper lobe. Contrast enhanced thin-section CT (**a**) and conventional T1-weighted SE (**b**) images suggest chest wall invasion. STIR turbo SE (**c**) image also clearly shows chest wall invasion and tumor extent

sagittal and coronal MR images are superior to CT for evaluating the local extent of disease in patients with superior sulcus tumors (Rapoport et al. 1988; Heelan et al. 1989; Webb et al. 1991; Padovani et al. 1993; Bonomo et al. 1996; Freundlich et al. 1996). Heelan et al. (1989) examined a series of 31 patients with superior sulcus tumors imaged with both CT and MR, and found that MR imaging showed 94% correlation with surgical and clinical findings, whereas the CT scans had an accuracy of only 63% for evaluating tumor invasion through the superior sulcus.

Sakai et al. (1997) used dynamic cine MR imaging during breathing rather than static MR imaging for evaluating chest wall invasion in lung cancer patients. This study evaluated the movement of the tumor along the parietal pleura during the respiratory cycle displayed with a cine loop in a manner similar to dynamic expiratory multi-section CT (Murata et al. 1994). Where the tumor had invaded the chest wall, it was fixed to the chest wall, while without invasion, the tumor was seen to move freely along the parietal pleura. In this study, the sensitivity, specificity, and accuracy of dynamic cine MR imaging for the detection of chest wall invasion were 100%, 70%, and 76%, respectively, and those of conventional CT and MR imaging were 80%, 65%, and 68% (Sakai et al. 1997). Of special significance is that the negative predictive value of dynamic cine MR imaging in this study was 100% without any need for ionizing radiation exposure. Dynamic cine MR imaging, when used in conjunction with static MR imaging, is therefore considered useful for further improvements of the assessment of chest wall invasion in lung cancer patients.

Currently, multiplanar capability, faster scan time and better spatial resolution of thin-section MDCT images may improve the diagnostic capability of CT for evaluation of chest wall invasion in NSCLC patients similar to that of mediastinal invasion. MR imaging is still considered to have superior tissue contrast compared with MDCT. Higashino et al. (2005) also reported that thin-section sagittal MPR imaging with 1 mm section thickness could significantly improve diagnostic accuracy for chest wall invasion in comparison with routine MDCT with 5 mm section thickness, and showed slightly better diagnostic capability than thin-section MDCT with 1 mm section thickness. Therefore, further investigations as well as comparative studies of thin-section MDCT imaging and MR imaging used as described here, or of newly developed techniques will be needed to determine the actual significance of MR imaging for assessment of chest wall invasion in routine clinical practice.

11.4.1.4 MR Assessment of Respiratory Tumor Motion

The general objective of radiotherapy is to achieve tumor control by depositing a lethal dose in the target volume including potential microscopic spread of cancer cells, while sparing surrounding organs and tissue as best as possible. Therefore, precise localization of the target volume is needed. Actually, the recent advances in radiotherapy, including intensity modulated radiotherapy, adaptive radiotherapy as well as image guided radiotherapy allows for strong improvement of the accuracy of irradiation treatment. However, patient motion and especially respiratory motion has become a major obstacle for achieving high precision radiotherapy. Currently, in classic radiotherapy for lung tumors, such motion is accounted for with a generic target volume expansion, not considering the individual patient breathing characteristics and the mobility of the individual tumor. However, it has been widely recognized that the motion pattern of lung tumors and the breathing cycles vary greatly among patients. This empiric approach includes all surrounding healthy tissues that pass the planned target volume at any time of the breathing cycle to create a safety margin. Within this margin even the additional normal tissues will be irradiated unnecessarily, causing tissue damage or limiting the dose delivered to the target. Therefore it is attractive to define an individual treatment plan by limiting the irradiated volume to certain positions of the tumor on its path during respiration (gated technique) or to follow its respiratory movement (tracking techniques) (Li et al. 2008). Hence, the ultimate objective for radiotherapy of moving targets is to localize precisely the target in space and time in order to achieve a higher dose to be applied to the target while the maximum dose to the normal tissue is reduced, particularly for critical adjacent organs at risk. The better the delineation between target and normal tissue the lower the probability of complications and the higher the chance for tumor control eventually enhanced by the possibility to even increase tumor control by delivering an additional radiation dose solely to the target. For dedicated treatment planning, respiratory-gated four-dimensional (4D) MRI could be used to exactly define tumor size and its three-dimensional displacement during respiration in a single examination. The fourth dimension beyond the 3D space is time, in which patient motion and the change of the position of the tumor will be recorded. Ideally, 4D MRI would not only encode tumor and organ motion information, but also provide time resolved 3D data sets with reduced motion artifacts.

Numerous MR-based investigations of lung and tumor motion in the literature have been limited to examining the motion in a single plane or in a small number of orthogonal planes through the tumor. Two non-coplanar image views provided critical motion characterization, while the most significant displacement was in the cranial-caudal direction (Shimizu et al. 2000). For this purpose, the MR sequences derived from cardiac imaging have been adapted for respiratory motion analysis. These sequences were compared, demonstrating that fast imaging with a free precession steady-state gradient-echo provided significantly higher SNR than any fast low angle shot technique, while the latter had an advantage in higher temporal resolution.

The correlation between external fiducial markers (coils) and the internal organ motion was also studied using single-slice 4D MRI (Plathow et al. 2005). The correlation coefficients in the three orthogonal directions for different breathing types (thoracic or abdominal) were about 0.8, similar in magnitude to 4D CT. This quantitative information indicates that external fiducial markers might be satisfactory for predicting organ motion.

Volumetric 4D MR imaging was not possible before the recent introduction of multi-channel parallel detection systems. Parallel acquisition improves the performance of MR imaging by over an order of magnitude compared to single-channel MR systems. The signal to noise ratio (SNR) is usually degraded when using multi-element coils for multichannel imaging. Consequently, some of the gain in acceleration is sacrificed in order to maintain image quality. Compared with single-slice imaging, which requires multiple slice directions to view the critical motions of the moving organ, the volumetric 4D technique catches the entire volume in a single acquisition. However, single-slice 4D MR imaging has a higher speed and can be used to study fast heart beating and forced breathing maneuvers. Further improvement of 4D MR imaging may employ the view-sharing technique using a variable sampling rate in k-space and shares elements between image sets, reducing the acquisition time by an appropriate approximation. This technique, combined with parallel imaging, allows for volumetric 4D MR imaging in respiratory motion studies. Then the acquisition time could be below 0.7 s for a 3D torso image using a 1.5-T MRI scanner.

Concluding, significant improvement in 4D MRI has been made in the last years. Nevertheless 4D radiation therapy is still in its early stages of development. Promising advances are expected. At this point in time 4D MRI of lung tumor motion will play a larger role.

11.4.2 MR Assessment of N Classification

The descriptor *N classification* refers to the presence or absence of regional lymph node metastases (Sobin and Wittekind 2002). The definitions are given in Table 11.4. In the absence of distant metastasis, locoregional lymph node spread will determine therapy and prognosis. For patients without positive lymph nodes (N0 disease) or with only intrapulmonary or hilar lymph nodes (N1 disease), direct resection remains standard therapy. In case of positive ipsilateral mediastinal lymph nodes (N2 disease), chemotherapy combined preoperatively with surgery or with concurrent or sequential radical radiotherapy is a legitimate choice (Martini et al. 1997; Vansteenkiste et al. 1998). If patients have contralateral mediastinal lymph node metastases (N3 disease), however, they are generally rejected for surgery but will receive non-surgical combination treatment.

CT has been the standard noninvasive modality for staging of lung cancer. Enlarged lymph nodes (i.e. with a short axis of more than 10 mm or a long axis of more than 15 mm) are considered to be metastatic. Although an increase in the size of mediastinal lymph nodes correlates with malignant involvement in patients with lung cancer, the sensitivity and specificity of this finding are not very high because lymph nodes can be enlarged due to infection or inflammation. In addition, small nodes can sometimes contain metastatic deposits. The RDOG reported that the sensitivity and specificity of CT for *N classification* were only 52% and 69%, respectively (Webb et al. 1991), while the corresponding values from the Leuven Lung Cancer Group (LLCG) were 69% and 71% (Dillemans et al. 1994). Due to the substantial limitation of CT for depicting mediastinal lymph node metastases, additional mediastinoscopy with biopsy is necessary for adequate assessment of hilar and mediastinal nodes (Glazer et al. 1984, 1985; Musset et al. 1986; Poon et al. 19987; Laurent et al. 1988; Webb et al. 1991, 1993; McLoud et al. 1992).

Since the 1990s, FDG-PET has been used for differentiation between metastatic and non-metastatic lymph nodes based on the biochemical mechanism of increased glucose metabolism or tumor cell duplication (Wahl et al. 1994; Patz et al. 1995; Boiselle et al. 1998; Higashi et al. 1998; Gupta et al. 2000). However, elevated glucose metabolism may occur secondary to tumor, infection or inflammation (Dewan et al. 1993; Patz et al. 1993), and spatial resolution in PET is inferior to that of CT and MR, so that the diagnostic capability of the FDG-PET imaging is limited (Gupta et al. 2000). A large number of prospective studies have compared the diagnostic capability of N stage assessment using CT and FDG-PET. A meta-analysis demonstrated that FDG-PET was significantly more accurate than CT for identifying lymph node involvement (Gould et al. 2003). In addition, the respective median sensitivity and specificity of CT were 61% (interquartile range, 50%–71%) and 79% (interquartile range, 66%–89%), but those of FDG-PET were 85% (interquartile range, 67%–91%) and 90% (interquartile range, 82%–96%) (Gould et al. 2003). Moreover, it has been suggested that FDG-PET is more sensitive but less specific when CT showed enlarged lymph nodes [median sensitivity, 100% (interquartile range, 90%–100%); median specificity, 78% (interquartile range, 68%–100%)] than when CT showed no lymph node enlargement [median sensitivity, 82% (interquartile range, 65%–100%); median specificity, 93% (interquartile range, 92%–100%]; $P = 0.002$)] (Gould et al. 2003).

Since the introduction of MR imaging for assessment of lung cancer, the criteria for tumor involvement within lymph nodes depend solely on lymph node size, and were very similar to CT criteria. In some cases, however, histological examination has shown that a normal-sized regional lymph node may have metastases, and that nodal enlargement can be due to reactive hyperplasia or other non-malignant conditions. The detectability of calcifications, which are indicative for a benign lesion, is also limited for MRI when compared with CT. The direct multiplanar capability of MR imaging, however, is an advantage for the detection of lymph nodes in areas that are sub-optimally imaged in the axial plane, such as in the aorto-pulmonary (AP) window and subcarinal regions (Webb et al. 1991; Boiselle et al. 1998).

Recently, cardiac- and/or respiratory-triggered conventional or black-blood STIR turbo SE imaging has been recommended for detection of metastatic tumors and metastatic lymph nodes (Fujimoto et al. 1995; Eustace et al. 1998; Takenaka et al. 2002; Ohno et al. 2004d, 2007c; Kawai et al. 2006). These novel sequences may make to quantitatively assess the signal intensity of lymph nodes by means of comparison with a 0.9% normal saline phantom (Takenaka et al. 2002; Ohno et al. 2004d, 2007c). The STIR turbo SE sequence is a simple sequence, which can be easily included in clinical protocols to yield net of T1- and T2-relaxation times. On STIR turbo SE images, metastatic lymph nodes exhibit high signal intensity and non-metastatic lymph nodes low signal intensity (Figs. 11.15 and 11.16). Several studies have reported that sensitivity, specificity and accuracy of quantitatively and qualitatively assessed

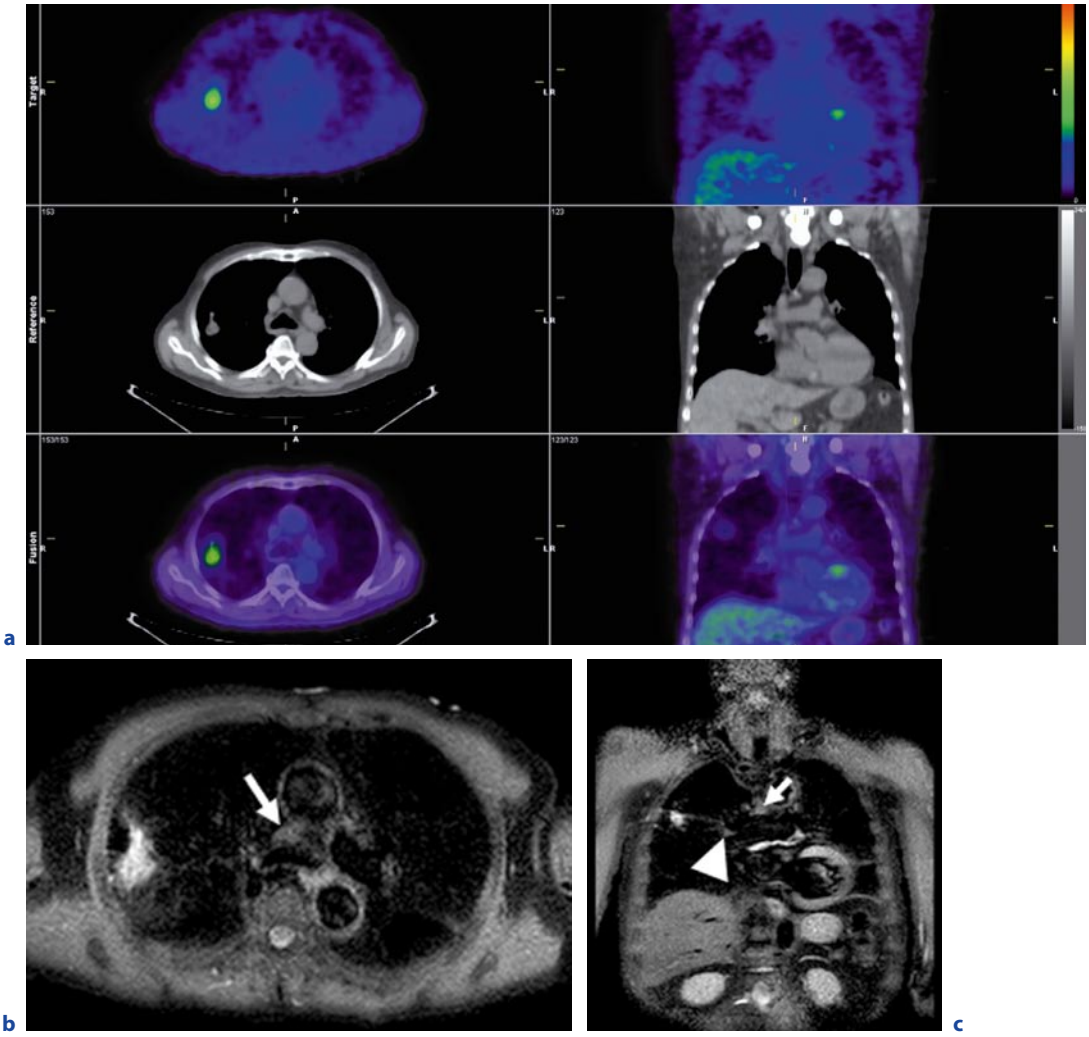

Fig. 11.15a–c. A 77-year-old male with adenocarcinoma (N0). Integrated FDG-PET/CT (**a**) demonstrates high uptake of FDG in primary tumor, but no uptake in mediastinal and hilar lymph nodes, suggesting N0. Black-blood STIR turbo SE imaging on axial (**b**) and coronal (**c**) planes show the primary tumor as high intensity, but mediastinal (*arrow*) and hilar (*arrow head*) lymph nodes as low signal intensity, suggesting N0

STIR turbo SE imaging ranged between 83.7% and 100.0%, between 75.0% and 93.1%, or between 86.0% and 92.2% on a per-patient basis (Fujimoto et al. 1995; Takenaka et al. 2002; Ohno et al. 2004d, 2007c). Direct and prospective comparisons with CT on a per-patient basis demonstrated that sensitivity and accuracy of quantitatively and qualitatively assessed STIR turbo SE imaging are significantly higher (Ohno et al. 2004d). In addition, direct and prospective comparisons with co-registered FDG-PET/CT showed that quantitative sensitivity and accuracy of STIR turbo SE imaging were significantly higher (Ohno et al. 2007c). STIR turbo SE imaging thus should be considered as capable of enhancing the diagnostic capability of *N classification* not only due to its multiplanar capability but also its sensitive and accurate assessment of relaxation time differences between metastatic and non-metastatic lymph nodes. It should therefore be considered at least as valuable as FDG-PET/CT. In fact, MR imaging with STIR turbo SE imaging may be discussed as a substitute for FDG-PET or PET/CT.

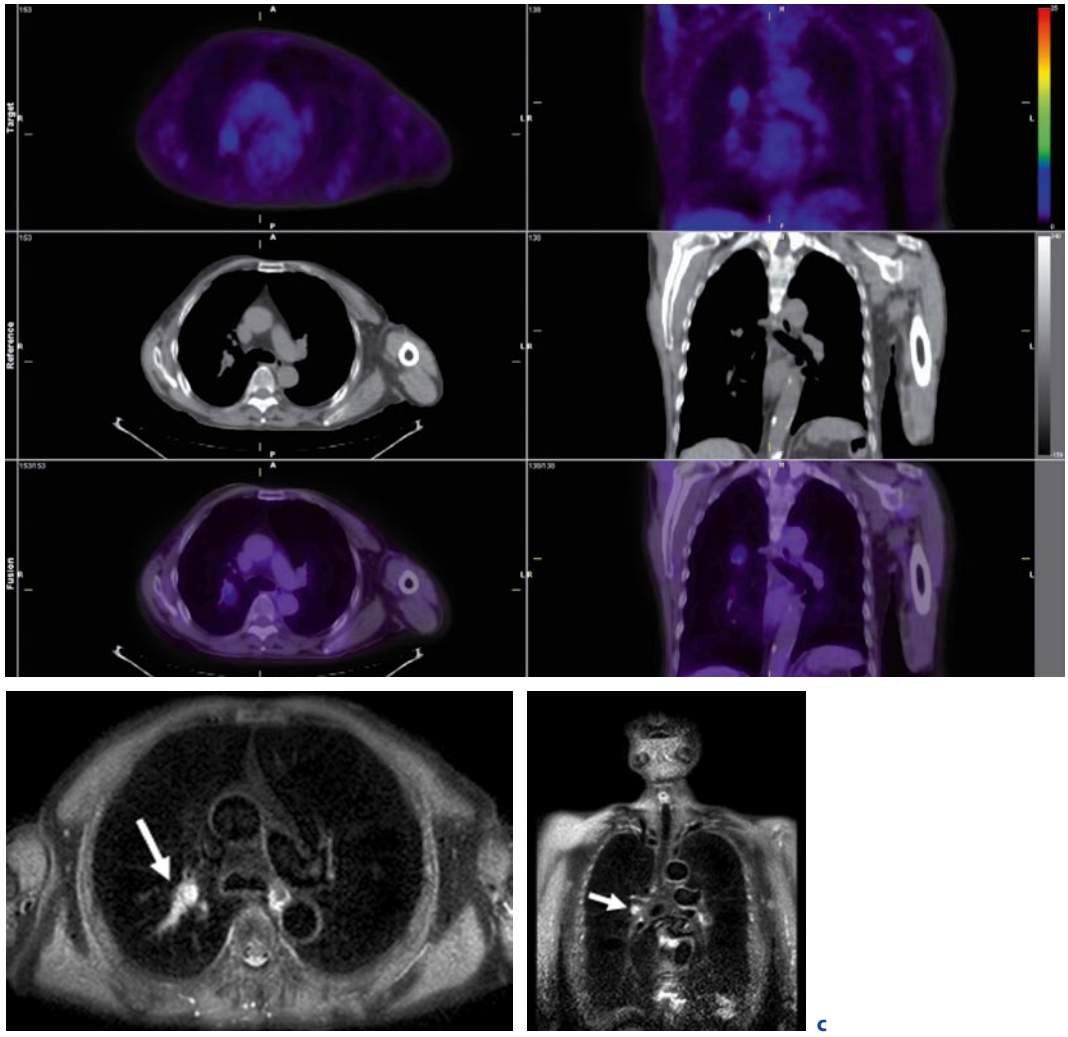

Fig. 11.16a–c. A 74-year-old male with adenocarcinoma (N1). Integrated FDG-PET/CT (**a**) demonstrates no uptake of FDG in the mediastinal and faint uptake in the hilar lymph nodes, suggesting N0, which was false-negative. Black-blood STIR turbo SE imaging on axial (**b**) and coronal (**c**) planes shows the hilar lymph node (*arrow*) as high signal intensity, suggesting N1 which was true-positive

11.4.3 MR Assessment of M Classification

The descriptor *M* relates to the presence of distant metastasis (M1) or its absence (M0) (Sobin and Wittekind 2002). The definitions are given in Table 11.5. Lung cancer can metastasize widely and involve many organs, including the brain, bone, liver, and adrenal glands. The presence of metastasis beyond the intrathoracic lymph nodes is considered an indication of metastatic disease (M1) and implies surgical non-resectability. Patients with distant metastases carry a very poor prognosis and are generally treated with chemotherapy, radiotherapy, or both or with optimal supportive care. In most cases, extrathoracic imaging is indicated for patients with lung cancer and symptoms localized to a specific organ. At present, however, there is no consensus regarding the efficacy of extrathoracic imaging for presumably resectable lung cancer without signs or symptoms localized to a specific organ (Wong et al. 1999).

The observation of metastases in patients with NSCLC has major implications for management and prognosis. Extrathoracic metastases are present in approximately 40% of patients with newly diagnosed lung cancer at presentation, most commonly in the adrenal glands, bones, liver, or brain (Pantel et al. 1996; Quint et al. 1996). After radical treatment for apparently localized disease, 20% of the patients developed an early distant relapse, probably due to systemic micrometastases that were present but not detected or visualized at the point of initial staging (Pantel et al. 1996). Silvestri et al. (1995) updated a meta-analysis for the systemic evaluation of extrathoracic metastases in potentially resectable NSCLC patients. This study calculated that the negative predictive value was equal to or more than 90% for the clinical evaluation of patients asymptomatic for brain, abdominal, or bone metastases (Silvestri et al. 1995). These findings are consistent with the findings of a retrospective analysis of 755 patients with clinical stage T1-2 N0 disease, which found only five sites with silent metastasis after extensive imaging for extrathoracic disease (Tanaka et al. 1999). The current recommendation from the American College of Chest Physicians (ACCP) therefore suggests that further diagnostic testing is necessary to confirm the presence of disease only in patients with abnormal findings on clinical evaluation, although the positive predictive values among the studies included in their meta-analysis were highly variable (Toloza et al. 2003; Silvestri et al. 2007). For purposes of TNM classification, however, it would be necessary to perform in-depth surveillance of potential sites of extra-thoracic metastases for all lung cancer patients. In addition, accurate diagnosis of extra-thoracic metastases may be helpful for clinicians to provide the most appropriate treatment and/or management for lung cancer patients.

11.4.3.1 Adrenal Gland Metastasis

Enlarged adrenal glands can be visualized on CT at initial presentation in nearly 10% of NSCLC patients, and approximately two-third of these adrenal lesions are benign or asymptomatic (Oliver et al. 1984; Ettinghausen and Burt 1991). Therefore, without pathologic proof of metastatic disease, the presence of an isolated adrenal mass in a patient with otherwise operable NSCLC should not preclude radical treatment. If the CT scan is performed without intravenous contrast media and an adrenal lesion is identified, measurement of the CT scan attenuation value can be helpful for distinguishing metastasis from adenoma (Boland et al. 1998; Szolar and Kammerhuber 1998). PET can also be a useful adjunct in this setting because the sensitivity and specificity of PET have been reported as ranging from 80% to 100% in the past literatures. This high sensitivity and specificity may result in a reduction of the number of unnecessary biopsies, which are not without risk and not always diagnostic (Erasmus et al. 1997; Marom et al. 1999). However, careful interpretation of PET is required for small lesions less than 10 mm in diameter, since experience with these is still limited (Schrevens et al. 2004). In addition, false-positive findings on PET have also been reported, and the incidence of false-positive findings is increasing. Currently, MR imaging is also considered helpful for distinguishing metastasis from adenoma when an adrenal lesion is detected by CT. Visual assessment of adrenal lesions using chemical shift MR imaging may characterize a lesion as an adenoma on the basis of reduced signal intensity of the lesion on opposed-phase images as compared with that on in-phase images (Korobkin et al. 1995; Schwartz et al. 1998; Hussain and Korobkin 2004). Korobkin et al. (1995) applied this technique to 51 adrenal lesions and reported a sensitivity of 100% and specificity of 81% for the characterization of adenomas.

11.4.3.2 Bone Metastasis

Bone involvement is usually assessed by 99mTechnetium methylene diphosphate (^{99m}Tc-MDP) or hydroxymethylene diphosphate (^{99m}Tc-HMDP) bone scintigraphy. Although sensitivity of bone scintigraphy has been reported as high as 90%, its specificity was only about 60% due to false-positive findings caused by the non-selective uptake of the radionuclide tracer in any area of increased bone turnover (Schrevens et al. 2004). Consequently, additional imaging by X-ray, bone CT, and/or MR imaging is often required. PET is reported to have similar sensitivity, but higher specificity and accuracy (equal to or more than 90%, equal to or more than 98% and equal to or more than 96%, respectively) (Bury et al. 1998; Marom et al. 1999). PET is therefore considered superior to bone scintigraphy for the detection of bone metastases. Currently, MR imaging with the use of various sequences such as T1-weighted SE or turbo SE imaging, T2-weighted turbo SE imaging, STIR turbo SE imaging, contrast-enhanced T1-weighted SE or turbo SE imaging, or diffusion-weighted MR imaging is deemed useful for assessment of muscle-skeletal tumors and metastasis from various malignancies

(Weinberger et al. 1995; Vanel et al. 1998; Mentzel et al. 2004; Park et al. 2004; Tokuda et al. 2004; Goo et al. 2005). However, only one study has directly compared the diagnostic capability of MR imaging and bone scintigraphy and found that sensitivity, specificity and accuracy of MR imaging were 80%, 96% and 93%, respectively, being superior to bone scintigraphy (40%, 92%, and 83%), although the difference was not significant (Earnest et al. 1999).

11.4.3.3 Brain Metastasis

Some investigators have reported that brain MR imaging is useful for evaluation of asymptomatic brain metastases in patients with operable lung cancer (Hillers et al. 1994; Earnest et al. 1999; Yokoi et al. 1999). FDG-PET is not suitable for the detection of brain metastases since the sensitivity of PET is low due to the high glucose uptake of normal surrounding brain tissue. CT and/or MR imaging remain the method of choice for screening brain metastases. Yokoi et al. (1999) compared the efficacy of MR imaging and CT scans of brain in 332 patients with potentially operable asymptomatic NSCLC. Within 12 months of diagnosis, brain metastases were detected in 7% of the patients in this series. Preoperatively, brain metastases were detected in 3.4% of the patients by MR imaging and in 0.6% of the patients by CT scans. Other investigators have reported on the utility of contrast-enhanced brain MR imaging and found a high prevalence of asymptomatic brain metastasis in 28% of patients identified with contrast-enhanced brain MR imaging (Earnest et al. 1999). These findings suggest that preoperative brain MR imaging may be effective for patients with lung cancer.

11.4.3.4 Whole-body MR Imaging for Assessment of M Classification in Lung Cancer Patients

Findings of a recent randomized trial suggest that the addition of whole-body FDG-PET scanning to a conventional workup can identify more patients with extra-thoracic metastases among those with suspected NSCLC (van Tinteren et al. 2002). However, recent advances in MR techniques such as fast imaging and moving table techniques make it possible to perform total body MR imaging. Its usefulness has been investigated in the staging of breast cancer and the search for primary lesions in patients with metastatic carcinoma from an unknown primary lesion (Eustace et al. 1998; Walker et al. 2000; Antoch et al. 2003; Lauenstein et al. 2004; Takahara et al. 2004; Goehde et al. 2005; Schmidt et al. 2006). It was concluded that total body MR imaging may constitute a single, cost-effective imaging test for patients with metastatic carcinoma from an unknown primary (Eustace et al. 1998; Walker et al. 2000; Antoch et al. 2003; Lauenstein et al. 2004; Takahara et al. 2004; Goehde et al. 2005; Schmidt et al. 2006). However, the potential of total body MR imaging for lung cancer staging has not yet been satisfactorily delineated. Ohno et al. (2007d) performed a direct comparison of the diagnostic capability of whole-body MR imaging and FDG-PET for the *M classification* (Fig. 11.17 and 11.18). They reported that the interobserver agreement for whole-body MR imaging was substantially, but not significantly better than for whole-body FDG-PET on a per-site basis and a per-patient basis (Ohno et al. 2007d). For assessment of head and neck metastases, sensitivity (84.6%) and accuracy (95.0%) of whole-body MR imaging were significantly higher than those of FDG-PET (15.4% and 89.1%, respectively) on a per-site basis (Ohno et al. 2007d). In addition, the specificity (96.1%) and accuracy (94.8%) of whole-body MR imaging for bone metastasis were significantly higher than those of FDG-PET (88.3% and 88.2%, respectively) on a per-site basis (Ohno et al. 2007d). However, when brain metastases were excluded from head and neck metastases, sensitivity, specificity and accuracy of whole-body MR imaging were not significantly different from those of FDG-PET, nor were they for diagnosis of thoracic, abdominal and pelvic metastases (Ohno et al. 2007d). In addition, when evaluation on a per-patient basis of *M classification* included brain metastases as head and neck metastases, accuracy (80.0%) of whole-body MR imaging was significantly better than that of FDG-PET (73.3%), while exclusion of brain metastases from head and neck metastases, resulted in no significant differences in sensitivity, specificity and accuracy between whole-body MR imaging and FDG-PET (Ohno et al. 2007d). Whole-body MR imaging is therefore an accurate diagnostic technique, and should be considered at least as effective as FDG-PET for M classification of lung cancer patients (Figs. 11.17 and 11.18). However, further investigations will be needed to determine the actual significance of whole-body MR imaging as a potential substitute for FDG-PET or PET/CT.

a

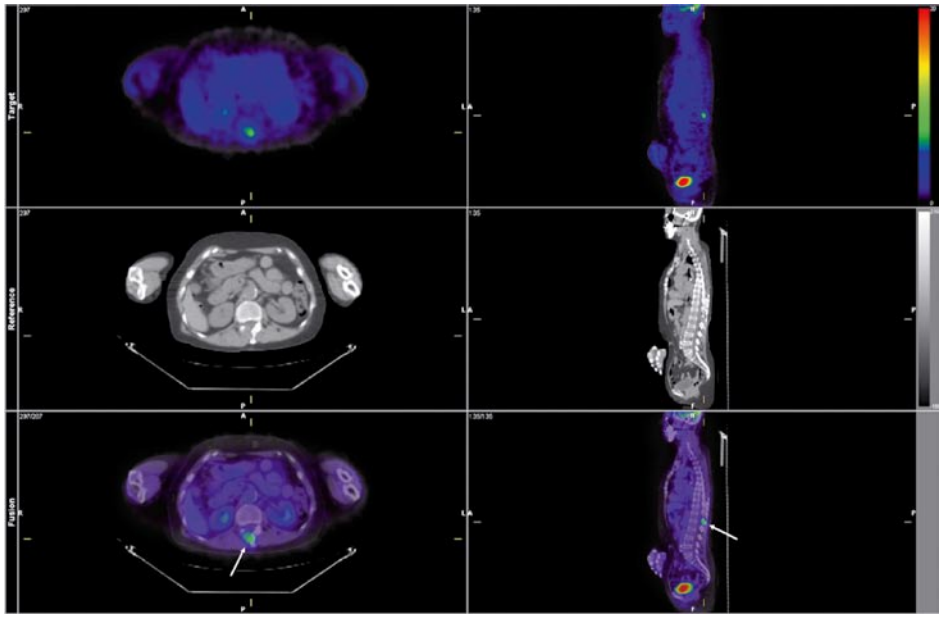

b

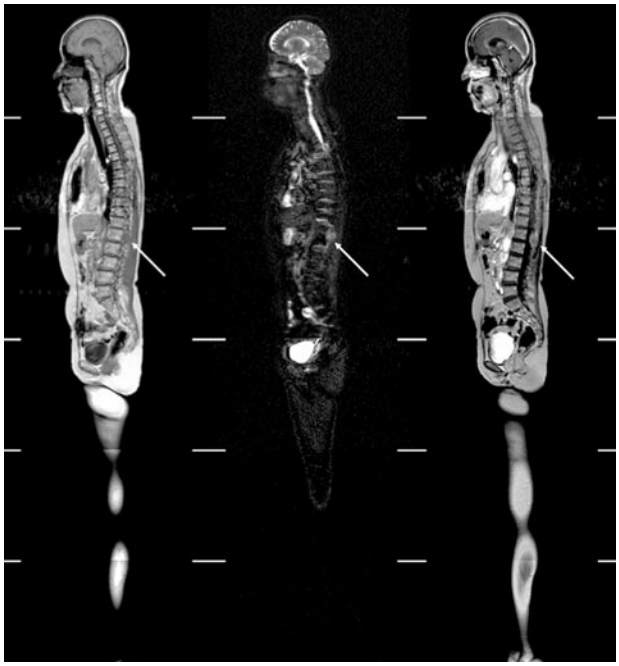

Fig. 11.17a,b. A 68-year-old female with adenocarcinoma and lumbar vertebra (L1) metastasis. Integrated FDG-PET/CT (**a**) shows high uptake of FDG at the vertebral arch (*arrow*), suggesting bone metastasis, which was true-positive. On sagittal whole-body MR images (**b**): L to R, non-contrast enhanced T1-weighted GRE image; STIR turbo SE image; and contrast enhanced T1-weighted GRE image, bone metastasis (*arrow*) is obvious, which was true-positive

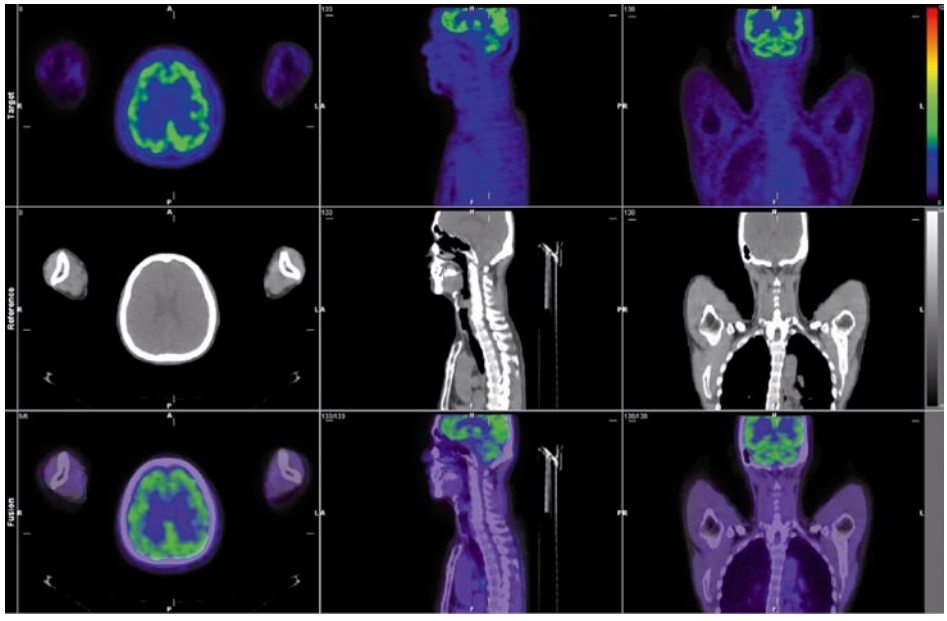

a

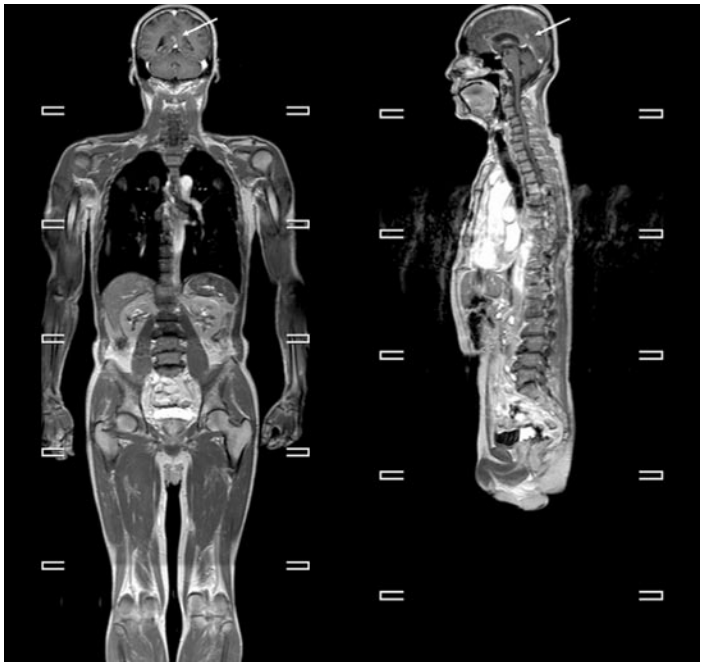

b

Fig. 11.18a,b. A 67-year-old male with adenocarcinoma and brain metastasis. Integrated FDG-PET/CT (**a**) does not show any abnormal uptake, and suggesting M0, which was false-negative. Contrast enhanced whole-body T1-weighted GRE (**b**): L to R, coronal and sagittal planes clearly shows brain metastasis, suggesting M1, which was true-positive

References

Amundsen T, Kvaerness J, Jones RA, Waage A, Bjermer L, Nilsen G, Haraldseth O (1997) Pulmonary embolism: detection with MR perfusion imaging of lung–a feasibility study. Radiology 203:181–185

Amundsen T, Torheim G, Waage A, Bjermer L, Steen PA, Haraldseth O (2000) Perfusion magnetic resonance imaging of the lung: characterization of pneumonia and chronic obstructive pulmonary disease. A feasibility study. J Magn Reson Imaging 12:224–231

Antoch G, Vogt FM, Freudenberg LS, Nazaradeh F, Goehde SC, Barkhausen J, Dahmen G, Bockisch A, Debatin JF, Ruehm SG (2003) Whole-body dual-modality PET/CT and whole-body MRI for tumor staging in oncology. JAMA 290:3199–3206

Aquino SL, Kee ST, Warnock ML, Gamsu G (1994) Pulmonary aspergillosis: imaging findings with pathologic correlation. AJR Am J Roentgenol 163:811–815

Armstrong P (2000) Neoplasms of the lung, airways and pleura. In: Armstrong P, Wilson AG, Dee P, Hansell DM (eds) Imaging of diseases of the chest, 3rd edn. Mosby, London, pp 305–401

Bach PB, Silvestri GA, Hanger M, Jett JR (2007) Screening for lung cancer: ACCP evidence-based clinical practice guidelines (2nd edition). American College of Chest Physicians. Chest 132:–69S–77S

Bailey PV, Tracy T Jr, Connors RH, deMello D, Lewis JE, Weber TR (1990) Congenital bronchopulmonary malformations. Diagnostic and therapeutic considerations. J Thorac Cardiovasc Surg 99:597–602

Baron RL, Levitt RG, Sagel SS, White MJ, Roper CL, Marbarger JP (1982) Computed tomography in the preoperative evaluation of bronchogenic carcinoma. Radiology 145:727–732

Bateson EM (1973) So-called hamartoma of the lung – a true neoplasm of fibrous connective tissue of the bronchi. Cancer 31:1458–1467

Blum U, Windfuhr M, Buitrago-Tellez C, Sigmund G, Herbst EW, Langer M (1994) Invasive pulmonary aspergillosis. MRI, CT, and plain radiographic findings and their contribution for early diagnosis Chest 106:1156–1161

Boiselle PM, Patz EF Jr, Vining DJ, Weissleder R, Shepard JA, McLoud TC (1998) Imaging of mediastinal lymph nodes: CT, MR, and FDG PET. Radiographics 18:1061–1069

Boland GW, Lee MJ, Gazelle GS, Halpern EF, McNicholas MM, Mueller PR (1998) Characterization of adrenal masses using unenhanced CT: an analysis of the CT literature. AJR Am J Roentgenol 171:201–204

Bonomo L, Ciccotosto C, Guidotti A, Storto ML (1996) Lung cancer staging: the role of computed tomography and magnetic resonance imaging. Eur J Radiol 23:35–45

Bourgouin PM, McLoud TC, Fitzgibbon JF, Mark EJ, Shepard JA, Moore EM, Rummeny E, Brady TJ (1991) Differentiation of bronchogenic carcinoma from postobstructive pneumonitis by magnetic resonance imaging: histopathologic correlation. J Thorac Imaging 6:22–27

Bruegel M, Gaa J, Woertler K, Ganter C, Waldt S, Hillerer C, Rummeny EJ (2007) MRI of the lung: value of different turbo spin-echo, single-shot turbo spin-echo, and 3D gradient-echo pulse sequences for the detection of pulmonary metastases. J Magn Reson Imaging 25:73–81

Bryant AS, Cerfolio RJ (2006) The maximum standardized uptake values on integrated FDG-PET/CT is useful in differentiating benign from malignant pulmonary nodules. Ann Thorac Surg 82:1016–1020

Bury T, Dowlati A, Paulus P, Corhay JL, Benoit T, Kayembe JM, Limet R, Rigo P, Radermecker M (1996) Evaluation of the solitary pulmonary nodule by positron emission tomography imaging. Eur Respir J 9:410–414

Bury T, Barreto A, Daenen F, Barthelemy N, Ghaye B, Rigo P (1998) Fluorine-18 deoxyglucose positron emission tomography for the detection of bone metastases in patients with non-small cell lung cancer. Eur J Nucl Med 25:1244–1247

Caskey CI, Templeton PA, Zerhouni EA (1990) Current evaluation of the solitary pulmonary nodule. Radiol Clin North Am 28:511–520

Chang JM, Lee HJ, Goo JM, Lee HY, Lee JJ, Chung JK, Im JG (2006) False positive and false negative FDG-PET scans in various thoracic diseases. Korean J Radiol 7:57–69

Christensen JA, Nathan MA, Mullan BP, Hartman TE, Swensen SJ, Lowe VJ (2006) Characterization of the solitary pulmonary nodule: 18F-FDG PET versus nodule-enhancement CT. AJR Am J Roentgenol 187:1361–1367

Chung MH, Lee HG, Kwon SS, Park SH (2000) MR imaging of solitary pulmonary lesion: emphasis on tuberculomas and comparison with tumors. J Magn Reson Imaging 11:629–637

Costello P (1994) Spiral CT of the thorax. Semin Ultrasound CT MR 15:90–106

Davis SD (1991) CT evaluation for pulmonary metastases in patients with extrathoracic malignancy. Radiology 180:1–12

Dewan NA, Gupta NC, Redepenning LS, Phalen JJ, Frick MP (1993) Diagnostic efficiency of PET-FDG imaging in solitary pulmonary nodules. Chest 104:997–1002

Dillemans B, Deneffe G, Verschakelen J, Decramer M (1994) Value of computed tomography and mediastinoscopy in preoperative evaluation of mediastinal nodes in non-small cell lung cancer. A study of 569 patients. Eur J Cardiothorac Surg 8:37–42

Donmez FY, Yekeler E, Saeidi V, Tunaci A, Tunaci M, Acunas G (2007) Dynamic contrast enhancement patterns of solitary pulmonary nodules on 3D gradient-recalled echo MRI. AJR Am J Roentgenol 189:1380–1386

Earnest F IV, Ryu JH, Miller GM, Luetmer PH, Forstrom LA, Burnett OL, Rowland CM, Swensen SJ, Midthun DE (1999) Suspected non-small cell lung cancer: incidence of occult brain and skeletal metastases and effectiveness of imaging for detection – pilot study. Radiology 211:137–145

Erasmus JJ, Patz EF Jr, McAdams HP, Murray JG, Herndon J, Coleman RE, Goodman PC (1997) Evaluation of adrenal masses in patients with bronchogenic carcinoma using 18F-fluorodeoxyglucose positron emission tomography. AJR Am J Roentgenol 168:1357–1360

Ettinghausen SE, Burt ME (1991) Prospective evaluation of unilateral adrenal masses in patients with operable non-small-cell lung cancer. J Clin Oncol 9:1462–1466

Eustace S, Tello R, DeCarvalho V, Carey J, Melhem E, Yucel EK (1998) Whole body turbo STIR MRI in unknown primary tumor detection. J Magn Reson Imaging 8:751–753

Felson B, Wiot JF (1977) Some less familiar roentgen manifestations of carcinoma of the lung. Semin Roentgenol 2:187–206

Feuerstein IM, Jicha DL, Pass HI, Chow CK, Chang R, Ling A, Hill SC, Dwyer AJ, Travis WD, Horowitz ME, Steinberg SM, Frank JA, Doppman JL (1992) Pulmonary metastases: MR imaging with surgical correlation – a prospective study. Radiology 182:123–129

Finck S, Milne EN (1988) A case report of segmental bronchial atresia: radiologic evaluation including computed tomography and magnetic resonance imaging. J Thorac Imaging 3:53–57

Fink C, Puderbach M, Bock M, Lodemann KP, Zuna I, Schmähl A, Delorme S, Kauczor HU (2004) Regional lung perfusion: assessment with partially parallel three-dimensional MR imaging. Radiology 231:175–184

Freundlich IM, Chasen MH, Varma DG (1996) Magnetic resonance imaging of pulmonary apical tumors. J Thorac Imaging 11:210–222

Fujimoto K, Meno S, Nishimura H, Hayabuchi N, Hayashi A (1994) Aspergilloma within cavitary lung cancer: MR imaging findings. AJR Am J Roentgenol 163:565–567

Fujimoto K, Edamitsu O, Meno S, Abe T, Honda N, Ogoh Y, Ohzono H, Nakaoda K, Kojima K, Nishimura H (1995) MR diagnosis for metastasis or non-metastasis of mediastinal and hilar lymph nodes in cases of primary lung cancer: detectability, signal intensity, and MR-pathologic correlation. Nippon Acta Radiol 55:162–171

Fujimoto K, Abe T, Müller NL, Terasaki H, Kato S, Sadohara J, Kono R, Edamitsu O, Ishitake T, Hayashi A, Rikimaru T, Hayabuchi N (2003) Small peripheral pulmonary carcinomas evaluated with dynamic MR imaging: correlation with tumor vascularity and prognosis. Radiology 227:786–793

Gaeta M, Blandino A, Scribano E, Vinci S, Minutoli F, Pergolizzi S, Pandolfo I (2000) Magnetic resonance imaging of bronchioloalveolar carcinoma. J Thorac Imaging 15:41–47

Gaeta M, Minutoli F, Ascenti G, Vinci S, Mazziotti S, Pandolfo I, Blandino A (2001) MR white lung sign: incidence and significance in pulmonary consolidations. J Comput Assist Tomogr 25:890–896

Gaeta M, Vinci S, Minutoli F, Mazziotti S, Ascenti G, Salamone I, Lamberto S, Blandino A (2002) CT and MRI findings of mucin-containing tumors and pseudotumors of the thorax: pictorial review. Eur Radiol 12:181–189

Gdeedo A, Van Schil P, Corthouts B, Van Mieghem F, Van Meerbeeck J, Van Marck E (1997) Comparison of imaging TNM [(i)TNM] and pathological TNM [pTNM] in staging of bronchogenic carcinoma. Eur J Cardiothorac Surg 12:224–227

Gefter WB (1992) The spectrum of pulmonary aspergillosis. J Thorac Imaging 7:56–74

Glazer GM, Orringer MB, Gross BH, Quint LE (1984) The mediastinum in non-small cell lung cancer: CT-surgical correlation. AJR Am J Roentgenol 142:1101–1105

Glazer GM, Gross BH, Aisen AM, Quint LE, Francis IR, Orringer MB (1985) Imaging of the pulmonary hilum: a prospective comparative study in patients with lung cancer. AJR Am J Roentgenol 145:245–248

Glazer HS, Kaiser LR, Anderson DJ, Molina PL, Emami B, Roper CL, Sagel SS (1989) Indeterminate mediastinal invasion in bronchogenic carcinoma: CT evaluation. Radiology 173:37–42

Goehde SC, Hunold P, Vogt FM, Ajaj W, Goyen M, Herborn CU, Forsting M, Debatin JF, Ruehm SG (2005) Full-body cardiovascular and tumor MRI for early detection of disease: feasibility and initial experience in 298 subjects. AJR Am J Roentgenol 184:598–611

Goo HW, Choi SH, Ghim T, Moon HN, Seo JJ (2005) Whole-body MRI of paediatric malignant tumours: comparison with conventional oncological imaging methods. Pediatr Radiol 35:766–773

Gould MK, Kuschner WG, Rydzak CE, Maclean CC, Demas AN, Shigemitsu H, Chan JK, Owens DK (2003) Test performance of positron emission tomography and computed tomography for mediastinal staging in patients with non-small-cell lung cancer: a meta-analysis. Ann Intern Med 139:879–892

Gückel C, Schnabel K, Deimling M, Steinbrich W (1996) Solitary pulmonary nodules: MR evaluation of enhancement patterns with contrast – enhanced dynamic snapshot gradient – echo imaging. Radiology 200:681–686

Gupta NC, Graeber GM, Bishop HA (2000) Comparative efficacy of positron emission tomography with fluorodeoxyglucose in evaluation of small (<1 cm), intermediate (1 to 3 cm), and large (>3 cm) lymph node lesions. Chest 117:773–778

Hatabu H, Gaa J, Kim D, Li W, Prasad PV, Edelman RR (1996) Pulmonary perfusion: qualitative assessment with dynamic contrast-enhanced MRI using ultra-short TE and inversion recovery turbo FLASH. Magn Reson Med 36:503–508

Hatabu H, Tadamura E, Levin DL, Chen Q, Li W, Kim D, Prasad PV, Edelman RR (1999) Quantitative assessment of pulmonary perfusion with dynamic contrast-enhanced MRI. Magn Reson Med 42:1033–1038

Heelan RT, Demas BE, Caravelli JF, Martini N, Bains MS, McCormack PM, Burt M, Panicek DM, Mitzner A (1989) Superior sulcus tumors: CT and MR imaging. Radiology 170:637–641

Henschke CI, McCauley DI, Yankelevitz DF, Naidich DP, McGuinness G, Miettinen OS, Libby D, Pasmantier M, Koizumi J, Altorki N, Smith JP (2001) Early lung cancer action project: a summary of the findings on baseline screening. Oncologist 6:147–152

Herder GJ, Golding RP, Hoekstra OS, Comans EF, Teule GJ, Postmus PE, Smit EF (2004) The performance of (18) F-fluorodeoxyglucose positron emission tomography in small solitary pulmonary nodules. Eur J Nucl Med Mol Imaging 31:1231–1236

Herman SJ, Winton TL, Weisbrod GL, Towers MJ, Mentzer SJ (1994) Mediastinal invasion by bronchogenic carcinoma: CT signs. Radiology 190:841–846

Herold CJ, Kramer J, Sertl K, Kalhs P, Mallek R, Imhof H, Tscholakoff D (1989) Invasive pulmonary aspergillosis: evaluation with MR imaging. Radiology 173:717–721

Higashi K, Nishikawa T, Seki H, Oguchi M, Nambu Y, Ueda Y, Yuasa K, Tonami H, Okimura T, Yamamoto I (1998) Comparison of fluorine-18-FDG PET and thallium-201 SPECT in evaluation of lung cancer. J Nucl Med 39:9–15

Higashino T, Ohno Y, Takenaka D, Watanabe H, Nogami M, Ohbayashi C, Yoshimura M, Satouchi M, Nishimura Y, Fujii M, Sugimura K (2005) Thin-section multiplanar reformats from multidetector-row CT data: utility for assessment of regional tumor extent in non-small cell lung cancer. Eur J Radiol 56:48–55

Hillers TK, Sauve MD, Guyatt GH (1994) Analysis of published studies on the detection of extrathoracic metastases in patients presumed to have operable non-small cell lung cancer. Thorax 49:14–19

Hittmair K, Eckersberger F, Klepetko W, Helbich T, Herold CJ (1995) Evaluation of solitary pulmonary nodules with dynamic contrast-enhanced MR imaging – a promising technique. Magn Reson Imaging 13:923–933

Hussain HK, Korobkin M (2004) MR imaging of the adrenal glands. Magn Reson Imaging Clin N Am 12:515–544

Jederlinic PJ, Sicilian LS, Baigelman W, Gaensler EA (1987) Congenital bronchial atresia. A report of 4 cases and a review of the literature. Medicine 66:73–83

Jeong YJ, Lee KS, Jeong SY, Chung MJ, Shim SS, Kim H, Kwon OJ, Kim S (2005) Solitary pulmonary nodule: characterization with combined wash-in and washout features at dynamic multi-detector row CT. Radiology 237:675–683

Joshi U, Raijmakers PG, van Lingen A, Comans EF, Pijpers R, Teule GJ, Hoekstra OS (2005) Evaluation of pulmonary nodules: comparison of a prototype dual crystal (LSO/NAI) dual head coincidence camera and full ring positron emission tomography (PET). Eur J Radiol 55:250–254

Kawai Y, Sumi M, Nakamura T (2006) Turbo short tau inversion recovery imaging for metastatic node screening in patients with head and neck cancer. AJNR Am J Neuroradiol 27:1283–1287

Kersjes W, Mayer E, Buchenroth M, Schunk K, Fouda N, Cagil H (1997) Diagnosis of pulmonary metastases with turbo-SE MR imaging. Eur Radiol 7:1190–1194

Kim SK, Allen-Auerbach M, Goldin J, Fueger BJ, Dahlbom M, Brown M, Czernin J, Schiepers C (2007) Accuracy of PET/CT in characterization of solitary pulmonary lesions. J Nucl Med 48:214–220

Ko SF, Lee TY, Kao CL, Ng SH, Wan YL, Lin JW, Chen WJ (1998) Bronchial atresia associated with epibronchial right pulmonary artery and aberrant right middle lobe artery.Br J Radiol 71:217–220

Kono M, Adachi S, Kusumoto M, Sakai E (1993) Clinical utility of Gd – DTPA - enhanced magnetic resonance imaging in lung cancer. J Thorac Imaging 8:18–26

Kono R, Fujimoto K, Terasaki H, Müller NL, Kato S, Sadohara J, Hayabuchi N, Takamori S (2007) Dynamic MRI of solitary pulmonary nodules: comparison of enhancement patterns of malignant and benign small peripheral lung lesions. AJR Am J Roentgenol 188:26–36

Korobkin M, Lombardi TJ, Aisen AM, Francis IR, Quint LE, Dunnick NR, Londy F, Shapiro B, Gross MD, Thompson NW (1995) Characterization of adrenal masses with chemical shift and gadolinium-enhanced MR imaging. Radiology 197:411–418

Kusumoto M, Kono M, Adachi S, Yamasaki K, Itouji E, Sakai E, Endo M, Nakamura T, Kimura K (1994) Gadopentetate dimeglumine – enhanced magnetic resonance imaging for lung nodules: differentiation of lung cancer and tuberculoma. Invest Radiol 29:S255–S256

Lauenstein TC, Goehde SC, Herborn CU, Goyen M, Oberhoff C, Debatin JF, Ruehm SG, Barkhausen J (2004) Whole-body MR imaging: evaluation of patients for metastases. Radiology 233:139–148

Laurent F, Drouillard J, Dorcier F, Velly JF, Barat JL, Grelet P, Martigne C, Tavernier J, Couraud L (1988) Bronchogenic carcinoma staging: CT versus MR imaging. Assessment with surgery. Eur J Cardiothorac Surg 2:31–36

Lee KS, Yi CA, Jeong SY, Jeong YJ, Kim S, Chung MJ, Kim HY, Kim YK, Lee KH (2007) Solid or partly solid solitary pulmonary nodules: their characterization using contrast wash-in and morphologic features at helical CT. Chest 131:1516–1525

Levin DL, Chen Q, Zhang M, Edelman RR, Hatabu H (2001) Evaluation of regional pulmonary perfusion using ultrafast magnetic resonance imaging. Magn Reson Med 46:166–171

Lewis JW Jr, Pearlberg JL, Beute GH, Alpern M, Kvale PA, Gross BH, Magilligan DJ Jr (1990) Can computed tomography of the chest stage lung cancer? Yes and no. Ann Thorac Surg 49:591–595

Li G, Citrin D, Camphausen K et al. (2008) Advances in 4D medical imaging and 4D radiation therapy. Technol Cancer Res Treat 7:67–81

Luboldt W, Wetter A, Eichler K, Vogl TJ, Wagner TO, Seemann MD (2006) Determination of the optimal MRI sequence for the detection of malignant lung nodules. Eur J Med Res 11:336–342

Ma H, Kubicek CP, Röhr M (1985) Metabolic effects of manganese deficiency in Aspergillus niger: evidence for increased protein degradation. Arch Microbiol 141:266–268

Magdeleinat P, Alifano M, Benbrahem C, Spaggiari L, Porrello C, Puyo P, Levasseur P, Regnard JF (2001) Surgical treatment of lung cancer invading the chest wall: results and prognostic factors. Ann Thorac Surg 71:1094–1099

Marom EM, McAdams HP, Erasmus JJ, Goodman PC, Culhane DK, Coleman RE, Herndon JE, Patz EF Jr (1999) Staging non-small cell lung cancer with whole-body PET. Radiology 212:803–809

Martini N, Heelan R, Westcott J, Bains MS, McCormack P, Caravelli J, Watson R, Zaman M (1985) Comparative merits of conventional, computed tomographic, and magnetic resonance imaging in assessing mediastinal involvement in surgically confirmed lung carcinoma. J Thorac Cardiovasc Surg 90:639–648

Martini N, Kris MG, Ginsberg RJ (1997) The role of multimodality therapy in locoregional non-small cell lung cancer. Surg Oncol Clin N Am 6:769–791

Matsuoka S, Uchiyama K, Shima H, Terakoshi H, Nojiri Y, Oishi S, Ogata H (2001) Detectability of pulmonary perfusion defect and influence of breath holding on contrast-enhanced thick-slice 2D and on 3D MR pulmonary perfusion images. J Magn Reson Imaging 14:580–585

Matsushima H, Takayanagi N, Satoh M, Kurashima K, Kanauchi T, Hoshi T, Kanazawa M (2002) Congenital bronchial atresia: radiologic findings in nine patients. J Comput Assist Tomogr 26:860–864

Mayr B, Heywang SH, Ingrisch H, Huber RM, Haussinger K, Lissner J (1987) Comparison of CT with MR imaging of endobronchial tumors. J Comput Assist Tomogr 11:43–48

McLoud TC, Swenson SJ (1999) Lung carcinoma. Clin Chest Med 20:97–713, vii

McLoud TC, Bourgouin PM, Greenberg RW, Kosiuk JP, Templeton PA, Shepard JA, Moore EH, Wain JC, Mathisen DJ, Grillo HC (1992) Bronchogenic carcinoma: analysis of staging in the mediastinum with CT by correlative lymph node mapping and sampling. Radiology 182:319–323

Meng RL, Jensik RJ, Faber LP, Matthew GR, Kittle CF (1978) Bronchial atresia. Ann Thorac Surg 25:184–192

Mentzel HJ, Kentouche K, Sauner D, Fleischmann C, Vogt S, Gottschild D, Zintl F, Kaiser WA (2004) Comparison of whole-body STIR-MRI and 99mTc-methylene-diphosphonate scintigraphy in children with suspected multifocal bone lesions. Eur Radiol 14:2297–2302

Mori K, Niki N, Kondo T, Kamiyama Y, Kodama T, Kawada Y, Moriyama N (2005) Development of a novel computer-aided diagnosis system for automatic discrimination of malignant from benign solitary pulmonary nodules on thin-section dynamic computed tomography. J Comput Assist Tomogr 29:215–222

Murata K, Takahashi M, Mori M, Shimoyama K, Mishina A, Fujino S, Itoh H, Morita R (1994) Chest wall and mediastinal invasion by lung cancer: evaluation with multisection expiratory dynamic CT. Radiology 191:251–255

Musset D, Grenier P, Carette MF, Frija G, Hauuy MP, Desbleds MT, Girard P, Bigot JM, Lallemand D (1986) Primary lung cancer staging: prospective comparative study of MR imaging with CT. Radiology 160:607–611

Naidich DP, Rumancik WM, Ettenger NA, Feiner HD, Harnanz-Schulman M, Spatz EM, Toder ST, Genieser NB (1988) Congenital anomalies of the lungs in adults: MR diagnosis. AJR Am J Roentgenol 151:13–19

Ohno Y, Adachi S, Kono M, Kusumoto M, Motoyama A, Sugimura K (2000) Predicting the prognosis of non-small cell lung cancer patient treated with conservative therapy using contrast-enhanced MR imaging. Eur Radiol 10:1770–1781

Ohno Y, Adachi S, Motoyama A, Kusumoto M, Hatabu H, Sugimura K, Kono M (2001) Multiphase ECG-triggered 3D contrast-enhanced MR angiography: utility for evaluation of hilar and mediastinal invasion of bronchogenic carcinoma. J Magn Reson Imaging 13:215–224

Ohno Y, Hatabu H, Takenaka D, Adachi S, Kono M, Sugimura K (2002) Solitary pulmonary nodules: potential role of dynamic MR imaging in management initial experience. Radiology 224:503–511

Ohno Y, Hatabu H, Takenaka D, Uematsu H, Ohbayashi C, Higashino T, Nogami M, Yoshimura M, Fujii M, Sugimura K (2004a) Dynamic MR imaging: value of differentiating subtypes of peripheral small adenocarcinoma of the lung. Eur J Radiol 52:144–150

Ohno Y, Hatabu H, Higashino T, Takenaka D, Watanabe H, Nishimura Y, Yoshimura M, Sugimura K (2004b) Dynamic perfusion MRI versus perfusion scintigraphy: prediction of postoperative lung function in patients with lung cancer. AJR Am J Roentgenol 182:73–78

Ohno Y, Hatabu H, Murase K, Higashino T, Kawamitsu H, Watanabe H, Takenaka D, Fujii M, Sugimura K (2004c) Quantitative assessment of regional pulmonary perfusion in the entire lung using three-dimensional ultrafast dynamic contrast-enhanced magnetic resonance imaging: preliminary experience in 40 subjects. J Magn Reson Imaging 20:353–365

Ohno Y, Hatabu H, Takenaka D, Higashino T, Watanabe H, Ohbayashi C, Yoshimura M, Satouchi M, Nishimura Y, Sugimura K (2004d) Metastases in mediastinal and hilar lymph nodes in patients with non-small cell lung cancer: quantitative and qualitative assessment with STIR turbo spin-echo MR imaging. Radiology 231:872–879

Ohno Y, Nogami M, Higashino T, Takenaka D, Matsumoto S, Hatabu H, Sugimura K (2005) Prognostic value of dynamic MR imaging for non-small-cell lung cancer patients after chemoradiotherapy. J Magn Reson Imaging 21:775–783

Ohno Y, Hatabu H, Murase K, Higashino T, Nogami M, Yoshikawa T, Sugimura K (2007a) Primary pulmonary hypertension: 3D dynamic perfusion MRI for quantitative analysis of regional pulmonary perfusion. AJR Am J Roentgenol 188:48–56

Ohno Y, Koyama H, Nogami M, Takenaka D, Matsumoto S, Yoshimura M, Kotani Y, Sugimura K (2007b) Postoperative lung function in lung cancer patients: comparative analysis of predictive capability of MRI, CT, and SPECT. AJR Am J Roentgenol 189:400–408

Ohno Y, Koyama H, Nogami M, Takenaka D, Yoshikawa T, Yoshimura M, Ohbayashi C, Sugimura K (2007c) STIR turbo SE MR imaging vs. coregistered FDG-PET/CT: quantitative and qualitative assessment of N-stage in non-small-cell lung cancer patients. J Magn Reson Imaging 26:1071–1080

Ohno Y, Koyama H, Nogami M, Takenaka D, Yoshikawa T, Yoshimura M, Kotani Y, Nishimura Y, Higashino T, Sugimura K (2007d) Whole-body MR imaging vs FDG-PET: comparison of accuracy of M-stage diagnosis for lung cancer patients. J Magn Reson Imaging 26:498–509

Oliver TW Jr, Bernardino ME, Miller JI, Mansour K, Greene D, Davis WA (1984) Isolated adrenal masses in nonsmall-cell bronchogenic carcinoma. Radiology 153:217–218

Padovani B, Mouroux J, Seksik L, Chanalet S, Sedat J, Rotomondo C, Richelme H, Serres JJ (1993) Chest wall invasion by bronchogenic carcinoma: evaluation with MR imaging. Radiology 187:33–38

Pantel K, Izbicki J, Passlick B, Angstwurm M, Häussinger K, Thetter O, Riethmüller G (1996) Frequency and prognostic significance of isolated tumour cells in bone marrow of patients with non-small-cell lung cancer without overt metastases. Lancet 347:649–653

Park SW, Lee JH, Ehara S, Park YB, Sung SO, Choi JA, Joo YE (2004) Single shot fast spin echo diffusion-weighted MR imaging of the spine; Is it useful in differentiating malignant metastatic tumor infiltration from benign fracture edema? Clin Imaging 28:102–108

Park Y, Kim TS, Yi CA, Cho EY, Kim H, Choi YS (2007) Pulmonary cavitary mass containing a mural nodule: differential diagnosis between intracavitary aspergilloma and cavitating lung cancer on contrast-enhanced computed tomography. Clin Radiol 62:227–232

Parmar H, Shah J, Patkar D, Varma R (2000) Intramedullary tuberculomas. MR findings in seven patients. Acta Radiol 41:572–577

Patz EF Jr, Lowe VJ, Hoffman JM, Paine SS, Burrowes P, Coleman RE, Goodman PC (1993) Focal pulmonary abnormalities: evaluation with F-18 fluorodeoxyglucose PET scanning. Radiology 188:487–490

Patz EF Jr, Lowe VJ, Goodman PC, Herndon J (1995) Thoracic nodal staging with PET imaging with 18FDG in patients with bronchogenic carcinoma. Chest 108:1617–1621

Plathow C, Zimmermann H, Fink C et al. (2005) Influence of different breathing maneuvers on internal and external organ motion: use of fiducial markers in dynamic MRI. Int J Rad Oncol Biol Phys 62:238–245

Poon PY, Bronskill MJ, Henkelman RM, Rideout DF, Shulman HS, Weisbrod GL, Steinhardt MI, Dunlap HJ, Ginsberg RJ, Feld R (1987) Mediastinal lymph node metastases from bronchogenic carcinoma: detection with MR imaging and CT. Radiology 162:651–656

Puderbach M, Risse F, Biederer J et al. (2008) In vivo Gd-DTPA concentration for MR lung perfusion measurements: assessment with computed tomography in a porcine model. Eur Radiol (in press)

Quint LE, Francis IR (1999) Radiologic staging of lung cancer. J Thorac Imaging 14:235–246

Quint LE, Glazer GM, Orringer MB (1987) Central lung masses: prediction with CT of need for pneumonectomy versus lobectomy. Radiology 165:735–738

Quint LE, Francis IR, Wahl RL, Gross BH, Glazer GM (1995) Preoperative staging of non-small-cell carcinoma of the lung: imaging methods. AJR Am J Roentgenol 164:1349–1359

Quint LE, Tummala S, Brisson LJ, Francis IR, Krupnick AS, Kazerooni EA, Iannettoni MD, Whyte RI, Orringer MB (1996) Distribution of distant metastases from newly diagnosed non-small cell lung cancer. Ann Thorac Surg 62:246–250

Rapoport S, Blair DN, McCarthy SM, Desser TS, Hammers LW, Sostman HD (1988) Brachial plexus: correlation of MR imaging with CT and pathologic findings. Radiology 167:161–165

Regier M, Kandel S, Kaul MG, Hoffmann B, Ittrich H, Bansmann PM, Kemper J, Nolte-Ernsting C, Heller M, Adam G, Biederer J (2007) Detection of small pulmonary nodules in high-field MR at 3 T: evaluation of different pulse sequences using porcine lung explants. Eur Radiol 17:1341–1351

Rendina EA, Bognolo DA, Mineo TC, Gualdi GF, Caterino M, Di Biasi C, Facciolo F, Ricci C (1987) Computed tomography for the evaluation of intrathoracic invasion by lung cancer. J Thorac Cardiovasc Surg 94:57–63

Sakai F, Sone S, Maruyama A, Kawai T, Imai S, Aoki J, Morimoto M, Haniuda M, Ueda H, Honda T (1992) Thin-rim enhancement in Gd-DTPA-enhanced magnetic resonance images of tuberculoma: a new finding of potential differential diagnostic importance. J Thorac Imaging 7:64–69

Sakai F, Sone S, Kiyono K, Maruyama A, Kawai T, Aoki J, Ueda H, Ishii K, Honda T, Morimoto M (1994) MR of pulmonary hamartoma: pathologic correlation. J Thorac Imaging 9:51–55

Sakai S, Murayama S, Murakami J, Hashiguchi N, Masuda K (1997) Bronchogenic carcinoma invasion of the chest wall: evaluation with dynamic cine MRI during breathing. J Comput Assist Tomogr 21:595–600

Schaefer JF, Vollmar J, Schick F, Vonthein R, Seemann MD, Aebert H, Dierkesmann R, Friedel G, Claussen CD (2004) Solitary pulmonary nodules: dynamic contrast-enhanced MR imaging – perfusion differences in malignant and benign lesions. Radiology 232:544–553

Schaefer JF, Schneider V, Vollmar J, Wehrmann M, Aebert H, Friedel G, Vonthein R, Schick F, Claussen CD (2006) Solitary pulmonary nodules: association between signal characteristics in dynamic contrast enhanced MRI and tumor angiogenesis. Lung Cancer 53:39–49

Schaefer-Prokop C, Prokop M (2002) New imaging techniques in the treatment guidelines for lung cancer. Eur Respir J Suppl 35:71s–83s

Schmidt GP, Haug AR, Schoenberg SO, Reiser MF (2006) Whole-body MRI and PET-CT in the management of cancer patients. Eur Radiol 16:1216–1225

Schrevens L, Lorent N, Dooms C, Vansteenkiste J (2004) The role of PET scan in diagnosis, staging, and management of non-small cell lung cancer. Oncologist 9:633–643

Schroeder T, Ruehm SG, Debatin JF, Ladd ME, Barkhausen J, Goehde SC (2005) Detection of pulmonary nodules using a 2D HASTE MR sequence: comparison with MDCT. AJR Am J Roentgenol 185:979–984

Schwartz LH, Ginsberg MS, Burt ME, Brown KT, Getrajdman GI, Panicek DM (1998) .MRI as an alternative to CT-guided biopsy of adrenal masses in patients with lung cancer. Ann Thorac Surg 65:193–197

Seo JS, Kim YJ, Choi BW, Choe KO (2005) Usefulness of magnetic resonance imaging for evaluation of cardiovascular invasion: evaluation of sliding motion between thoracic mass and adjacent structures on cine MR images. J Magn Reson Imaging 22:234–241

Shimizu S, Shirato H, Aoyama H et al. (2000) High-speed magnetic resonance imaging for four-dimensional treatment planning of conformal radiation therapy of moving body tumors. Int J Rad Oncol Biol Phys 48:471–474

Siegelman SS, Khouri NF, Scott WW Jr, Leo FP, Hamper UM, Fishman EK, Zerhouni EA (1986) Pulmonary hamartoma: CT findings. Radiology 160:313–317

Silvestri GA, Littenberg B, Colice GL (1995) The clinical evaluation for detecting metastatic lung cancer. A meta-analysis. Am J Respir Crit Care Med 152:225–230

Silvestri GA, Gould MK, Margolis ML, Tanoue LT, McCrory D, Toloza E, Detterbeck F, (2007) Noninvasive staging of non-small cell lung cancer: ACCP evidenced-based clinical practice guidelines, 2nd edn. American College of Chest Physicians. Chest 132:178S–201S

Sobin L, Wittekind Ch (2002) Lung cancer. In: Sobin L, Wittekind Ch (eds) TNM classification of malignant tumors, 6th edn. Wiley-Liss, New York, pp 99–103

Sochocky S (1958) Tuberculoma of the lung. Am Rev Tuber 78:403–410

Suzuki N, Saitoh T, Kitamura S (1993) Tumor invasion of the chest wall in lung cancer: diagnosis with US. Radiology 187:39–42

Swensen SJ, Morin RL, Schueler BA, Brown LR, Cortese DA, Pairolero PC, Brutinel WM (1992) Solitary pulmonary nodule: CT evaluation of enhancement with iodinated contrast media – a preliminary report. Radiology 182:343–347

Swensen SJ, Brown LR, Colby TV, Weaver AL, Midthum DE (1996) Lung nodule enhancement at CT: prospective findings. Radiology 201:447–455

Swensen SJ, Viggiano RW, Midthun DE, Müller NL, Sherrick A, Yamashita K, Naidich DP, Patz EF, Hartman TE, Muhm JR, Weaver AL (2000) Lung nodule enhancement at CT: multicenter study. Radiology 214:73–80

Swensen SJ, Jett JR, Hartman TE, Midthun DE, Mandrekar SJ, Hillman SL, Sykes AM, Aughenbaugh GL, Bungum AO, Allen KL (2005) CT screening for lung cancer: five-year prospective experience. Radiology 235:259–265

Szolar DH, Kammerhuber FH (1998) Adrenal adenomas and nonadenomas: assessment of washout at delayed contrast-enhanced CT. Radiology 207:369–375

Takahara T, Imai Y, Yamashita T, Yasuda S, Nasu S, Van Cauteren M (2004) Diffusion weighted whole body imaging with background body signal suppression (DWIBS): technical improvement using free breathing, STIR and high resolution 3D display. Radiat Med 22:275–282

Takahashi K, Furuse M, Hanaoka H, Yamada T, Mineta M, Ono H, Nagasawa K, Aburano T (2000) Pulmonary vein and left atrial invasion by lung cancer: assessment by breath-hold gadolinium-enhanced three-dimensional MR angiography. J Comput Assist Tomog 24:557–561

Takahashi M, Shimoyama K, Murata K, Mori M, Nitta N, Mishina A, Matsuo H, Morita R, Fujino S, Inoue S, Kato H (1997) Hilar and mediastinal invasion of bronchogenic carcinoma: evaluation by thin-section electron-beam computed tomography. J Thorac Imaging 12:195–199

Takenaka D, Ohno Y, Hatabu H, Ohbayashi C, Yoshimura M, Ohkita Y, Sugimura K (2002) Differentiation of metastatic versus non-metastatic mediastinal lymph nodes in patients with non-small cell lung cancer using respiratory-triggered short inversion time inversion recovery (STIR) turbo spin-echo MR imaging. Eur J Radiol 44:216–224

Tanaka K, Kubota K, Kodama T, Nagai K, Nishiwaki Y (1999) Extrathoracic staging is not necessary for non-small-cell lung cancer with clinical stage T1-2 N0. Ann Thorac Surg 68:1039–1042

Therasse P, Arbuck SG, Eisenhauer EA, Wanders J, Kaplan RS, Rubinstein L, Verweij J, Van Glabbeke M, van Oosterom AT, Christian MC, Gwyther SG (2000) New guidelines to evaluate the response to treatment in solid tumors. J Natl Cancer Inst 92:205–216

Tokuda O, Hayashi N, Matsunaga N (2004) MRI of bone tumors: Fast STIR imaging as a substitute for T1-weighted contrast-enhanced fat-suppressed spin-echo imaging. J Magn Reson Imaging 19:475–481

Toloza EM, Harpole L, McCrory DC (2003) Noninvasive staging of non-small cell lung cancer: a review of the current evidence. Chest 123:137S–146S

Tuddenham WJ (1984) Glossary of terms for thoracic radiology: recommendations of the Nomenclature Committee of the Fleischner Society. AJR Am J Roentgenol 143:509–517

van der Heide S, Kauffman HF, de Vries K (1985) Cultivation of fungi in synthetic and semi-synthetic liquid medium. II. Immunochemical properties of the antigenic and allergenic extracts. Allergy 40:592–598

van Tinteren H, Hoekstra OS, Smit EF, van den Bergh JH, Schreurs AJ, Stallaert RA, van Velthoven PC, Comans EF, Diepenhorst FW, Verboom P, van Mourik JC, Postmus PE, Boers M, Teule GJ (2002) Effectiveness of positron emission tomography in the preoperative assessment of patients with suspected non-small-cell lung cancer: the PLUS multicentre randomised trial. Lancet 359:1388–1393

Vanel D, Bittoun J, Tardivon A (1998) MRI of bone metastases. Eur Radiol 8:1345–1351

Vansteenkiste J, De Leyn P, Deneffe G, Menten J, Lerut T, Demedts M (1998) Present status of induction treatment in stage IIIA-N2 non-small cell lung cancer: a review. The Leuven Lung Cancer Group. Eur J Cardiothorac Surg 13:1–12

Vogt FM, Herborn CU, Hunold P, Lauenstein TC, Schröder T, Debatin JF, Barkhausen J (2004) HASTE MRI versus chest radiography in the detection of pulmonary nodules: comparison with MDCT. AJR Am J Roentgenol 183:71–78

Wahl RL, Quint LE, Greenough RL, Meyer CR, White RI, Orringer MB (1994) Staging of mediastinal non-small cell lung cancer with FDG PET, CT, and fusion images: preliminary prospective evaluation. Radiology 191:371–377

Walker R, Kessar P, Blanchard R, Dimasi M, Harper K, DeCarvalho V, Yucel EK, Patriquin L, Eustace S (2000) Turbo STIR magnetic resonance imaging as a whole-body screening tool for metastases in patients with breast carcinoma: preliminary clinical experience. J Magn Reson Imaging 11:343–350

Watanabe A, Shimokata K, Saka H, Nomura F, Sakai S (1991) Chest CT combined with artificial pneumothorax: value in determining origin and extent of tumor. AJR Am J Roentgenol 156:707–710

Webb WR, Gatsonis C, Zerhouni EA, Heelan RT, Glazer GM, Francis IR, McNeil BJ (1991) CT and MR imaging in staging non-small cell bronchogenic carcinoma: report of the Radiologic Diagnostic Oncology Group. Radiology 178:705–713

Webb WR, Sarin M, Zerhouni EA, Heelan RT, Glazer GM, Gatsonis C (1993) Interobserver variability in CT and MR staging of lung cancer. J Comput Assist Tomogr 17:841–846

Weinberger E, Shaw DW, White KS, Winters WD, Stark JE, Nazar-Stewart V, Hinks RS (1995) Nontraumatic pediatric musculoskeletal MR imaging: comparison of conventional and fast-spin-echo short inversion time inversion-recovery technique. Radiology 194:721–726

White CS (1996) MR evaluation of the pericardium and cardiac malignancies. Magn Reson Imaging Clin N Am 4:237–251

White PG, Adams H, Crane MD, Butchart EG (1994) Preoperative staging of carcinoma of the bronchus: can computed tomographic scanning reliably identify stage III tumours? Thorax 49:951–957

Wong J, Haramati LB, Rozenshtein A, Yanez M, Austin JH (1999) Non-small-cell lung cancer: practice patterns of extrathoracic imaging. Acad Radiol 6:211–215

World Health Organization (1979) WHO handbook for reporting the results of cancer treatment. World Health Organization, Geneva, Switzerland

Yamashita K, Matsunobe S, Tsuda T, Nemoto T, Matsumoto K, Miki H, Konishi J (1995) Solitary pulmonary nodules: preliminary study of evaluation with incremental dynamic CT. Radiology 194:399–405

Yi CA, Lee KS, Kim EA, Han J, Kim H, Kwon OJ, Jeong YJ, Kim S (2004) Solitary pulmonary nodules: dynamic enhanced multi-detector row CT study and comparison with vascular endothelial growth factor and microvessel density. Radiology 233:191–199

Yi CA, Lee KS, Kim BT, Choi JY, Kwon OJ, Kim H, Shim YM, Chung MJ (2006) Tissue characterization of solitary pulmonary nodule: comparative study between helical dynamic CT and integrated PET/CT. J Nucl Med 47:443–450

Yi CA, Jeon TY, Lee KS, Lee JH, Seo JB, Kim YK, Chung MJ (2007) 3-T MRI: usefulness for evaluating primary lung cancer and small nodules in lobes not containing primary tumors. AJR Am J Roentgenol 189:386–392

Yilmaz S, Ekici A, Erdogan S, Ekici M (2004) Endobronchial lipomatous hamartoma: CT and MR imaging features. Eur Radiol 14:1521–1524

Yokoi K, Mori K, Miyazawa N, Saito Y, Okuyama A, Sasagawa M (1991) Tumor invasion of the chest wall and mediastinum in lung cancer: evaluation with pneumothorax CT. Radiology 181:147–152

Yokoi K, Kamiya N, Matsuguma H, Machida S, Hirose T, Mori K, Tominaga K (1999) Detection of brain metastasis in potentially operable non-small cell lung cancer: a comparison of CT and MRI. Chest 115:714–719

Zhang M, Kono M (1997) Solitary pulmonary nodules: evaluation of blood flow patterns with dynamic CT. Radiology 205:471–4788

Zinreich SJ, Kennedy DW, Malat J, Curtin HD, Epstein JI, Huff LC, Kumar AJ, Johns ME, Rosenbaum AE (1988) Fungal sinusitis: diagnosis with CT and MR imaging. Radiology 169:439–444